A&A 614, A56 (2018)
https://doi.org/10.1051/0004-6361/201732407

Astronomy & Astrophysics

A Virgo Environmental Survey Tracing Ionised Gas Emission (VESTIGE)

I. Introduction to the survey⋆

A. Boselli[1], M. Fossati[2,3], L. Ferrarese[4], S. Boissier[4], G. Consolandi[5,6], A. Longobardi[7], P. Amram[1], M. Balogh[8], P. Barmby[9], M. Boquien[10], F. Boulanger[11], J. Braine[12], V. Buat[1], D. Burgarella[1], F. Combes[13,14], T. Contini[15], L. Cortese[16], P. Côté[4], S. Côté[4], J. C. Cuillandre[17], L. Drissen[18], B. Epinat[1], M. Fumagalli[19], S. Gallagher[8], G. Gavazzi[5], J. Gomez-Lopez[1], S. Gwyn[4], W. Harris[20], G. Hensler[21], B. Koribalski[22], M. Marcelin[1], A. McConnachie[4], M. A. Miville-Deschenes[11], J. Navarro[23], D. Patton[24], E. W. Peng[7,25], H. Plana[26], N. Prantzos[27], C. Robert[18], J. Roediger[4], Y. Roehlly[28], D. Russeil[1], P. Salome[12], R. Sanchez-Janssen[29], P. Serra[30], K. Spekkens[31,32], M. Sun[33], J. Taylor[8], S. Tonnesen[34], B. Vollmer[35], J. Willis[23], H. Wozniak[36], T. Burdullis[37], D. Devost[37], B. Mahoney[37], N. Manset[37], A. Petric[37], S. Prunet[37], and K. Withington[37]

(Affiliations can be found after the references)

Received 4 December 2017 / Accepted 7 February 2018

ABSTRACT

The Virgo Environmental Survey Tracing Ionised Gas Emission (VESTIGE) is a blind narrow-band (NB) $H\alpha$+[NII] imaging survey carried out with MegaCam at the Canada–France–Hawaii Telescope. The survey covers the whole Virgo cluster region from its core to one virial radius (104 deg^2). The sensitivity of the survey is of $f(H\alpha) \sim 4 \times 10^{-17}$ erg s^{-1} cm^{-2} (5σ detection limit) for point sources and $\Sigma(H\alpha) \sim 2 \times 10^{-18}$ erg s^{-1} cm^{-2} arcsec^{-2} (1σ detection limit at 3 arcsec resolution) for extended sources, making VESTIGE the deepest and largest blind NB survey of a nearby cluster. This paper presents the survey in all its technical aspects, including the survey design, the observing strategy, the achieved sensitivity in both the NB $H\alpha$+[NII] and in the broad-band r filter used for the stellar continuum subtraction, the data reduction, calibration, and products, as well as its status after the first observing semester. We briefly describe the $H\alpha$ properties of galaxies located in a 4×1 deg^2 strip in the core of the cluster north of M87, where several extended tails of ionised gas are detected. This paper also lists the main scientific motivations for VESTIGE, which include the study of the effects of the environment on galaxy evolution, the fate of the stripped gas in cluster objects, the star formation process in nearby galaxies of different type and stellar mass, the determination of the $H\alpha$ luminosity function and of the $H\alpha$ scaling relations down to $\sim 10^6\,M_\odot$ stellar mass objects, and the reconstruction of the dynamical structure of the Virgo cluster. This unique set of data will also be used to study the HII luminosity function in hundreds of galaxies, the diffuse $H\alpha$+[NII] emission of the Milky Way at high Galactic latitude, and the properties of emission line galaxies at high redshift.

Key words. galaxies: clusters: general – galaxies: clusters: individual: Virgo – galaxies: evolution – galaxies: interactions – galaxies: ISM

1. Introduction

Understanding the formation and evolution of galaxies remains a primary goal of modern astrophysics. The study of large samples of galaxies detected in wide field, multifrequency, ground- and space-based surveys, both in the local Universe (SDSS – York et al. 2000, GALEX – Martin et al. 2005, 2MASS – Skrutskie et al. 2006, ALFALFA – Giovanelli et al. 2005, HIPASS – Meyer et al. 2004, NVSS – Condon et al. 1998, WISE – Wright et al. 2010, all sky surveys) and at high redshift, has led to significant progress towards an understanding of the process of galaxy evolution. The sensitivity and both angular and spectral resolutions of the multifrequency data obtained in the most recent surveys have been fundamental in tracing the physical properties of different galaxy components; for example, stellar populations, gas in its different phases (cold atomic and molecular, ionised, hot), heavy elements (metals and dust), and dark matter, whose content and distribution are tightly connected to the evolutionary state of galaxies (e.g. Boselli 2011). These achievements have been mirrored by advances in the speed and precision of numerical methods used to simulate the formation of structures over wide ranges in mass and radius (e.g. Vogelsberger et al. 2014; Genel et al. 2014; Schaye et al. 2015; Crain et al. 2015).

Both observations and simulations consistently point to two main factors as key drivers of galaxy evolution: the secular evolution mainly driven by the dynamical mass of the system (e.g. Cowie et al. 1996; Gavazzi et al. 1996; Boselli et al. 2001) and the environment in which galaxies reside (Dressler 1980; Dressler et al. 1997; Balogh et al. 2000; Kauffmann et al. 2004; Boselli & Gavazzi 2006, 2014; Peng et al. 2010). The relative importance

⋆ Based on observations obtained with MegaPrime/MegaCam, a joint project of CFHT and CEA/DAPNIA, at the Canada–France–Hawaii Telescope (CFHT) which is operated by the National Research Council (NRC) of Canada, the Institut National des Sciences de l'Univers of the Centre National de la Recherche Scientifique (CNRS) of France and the University of Hawaii.

of these two factors over cosmic timescales for systems of different mass and type, however, remains elusive. Further progress hinges on the characterisation of astrophysical processes that are not fully understood at the present time: for example, cold gas accretion from filaments, gas dynamics, radiative cooling, star formation, stellar/AGN feedback, as well as all the possible effects induced by the interaction of galaxies with their surrounding environments.

The distribution of galaxies in the Universe is highly inhomogeneous, with densities spanning several orders of magnitude. If ρ_0 is the average field density, the density varies from $\sim 0.2\rho_0$ in voids to $\sim 5\rho_0$ in superclusters and filaments, $\sim 100\rho_0$ in the core of rich clusters, and up to $\sim 1000\rho_0$ in compact groups (Geller & Huchra 1989). Although containing only ∼5% of the local galaxies, clusters are ideal laboratories to study the physical mechanisms perturbing galaxy evolution in dense environments. Because of their high density, gravitational interactions between cluster members are expected to be frequent. At the same time, clusters are characterised by a hot ($T \sim 10^7$–10^8 K) and dense ($\rho_{\rm ICM} \sim 10^{-3}$ cm^{-3}) intracluster medium (ICM) trapped within their potential well (e.g. Sarazin 1986). The interaction of galaxies with this diffuse ICM can easily remove their interstellar medium, thus affecting their star formation activity.

Environmental processes can be broadly separated into two classes: those related to the gravitational interactions between galaxies or with the potential well of over-dense regions (merging – Kauffmann et al. 1993; tidal interactions – Merritt 1983; Byrd & Valtonen 1990; harassment – Moore et al. 1998), and those exerted by the hot and dense ICM on galaxies moving at high velocity within clusters (ram pressure stripping – Gunn & Gott 1972; viscous stripping – Nulsen 1982; thermal evaporation – Cowie & Songaila 1977; starvation – Larson et al. 1980). Since the large, dynamically-bounded structures observed in the local Universe form through the accretion of smaller groups of galaxies (Gnedin 2003; McGee et al. 2009; De Lucia et al. 2012), environmental processes are now believed to influence galaxies even before they enter rich clusters in the high-redshift Universe (pre-processing – Dressler 2004). This unexpected discovery has spawned a renewed interest in the detailed properties of galaxies in the local Universe, since such systems are the obvious test-beds for theories that attempt to explain this cosmic evolution. Indeed, studies of the high-redshift Universe can give us an integrated, statistical picture of galaxy evolution over cosmic time, but it is only through detailed studies of the local volume that we can hope to understand the detailed role of gas dynamics, cooling, star formation, feedback and environment in the hierarchical assembly of baryonic substructures.

Because of its proximity (16.5 Mpc), the Virgo cluster has been an ideal target for the study of the transformation of galaxies in rich environments. The first blind photographic survey of the cluster, led by A. Sandage, G. Tammann and B. Binggeli, was possible only after the construction of the 2.5 m (100-inch) Irénée du Pont telescope at Las Campanas (Chile) in 1977. The telescope was expressly designed to have an exceptionally wide field for direct photography ($1.5^\circ \times 1.5^\circ$) and was thus perfectly tuned to cover the whole Virgo cluster region. Only recently, the advent of the new generation of large panoramic detectors made it possible to cover the whole cluster, which exceeds 100 deg^2, from the UV to the radio wavelengths.

The studies of emission lines, however, which for wide-field cameras require specific and expensive narrow-band (NB) filters of large physical size, have thus far been limited to pointed observations. Very deep $H\alpha$ observations of a few galaxies in nearby clusters, including our recent observations with MegaCam, have led to several intriguing discoveries. They have shown that the ionised phase appears to be an ideal tracer of stripped gas in dense regions: approximately 50% of late-type galaxies show extended (∼50 kpc) tails of ionised gas with surface brightness $\Sigma(H\alpha)$ of approximately a few 10^{-18} erg s^{-1} cm^{-2} arcsec^{-2} (Boselli & Gavazzi 2014), while only a handful of galaxies have extended cold or hot gaseous tails (Chung et al. 2007; Sun et al. 2006, 2007, 2010; Scott et al. 2012; Sivanandam et al. 2014; Jáchym et al. 2014). In some objects, the cometary shape of the tails indicates that the gas has been stripped by the interaction with the hot ICM (Gavazzi et al. 2001; Yoshida et al. 2002; Yagi et al. 2010; Fossati et al. 2012, 2016, 2018 – paper II; Zhang et al. 2013; Boselli et al. 2016a); in other systems, bridges of ionised gas linking different nearby galaxies are associated with tidal tails in the stellar component, suggesting gravitational perturbations with nearby companions or within infalling groups (i.e. pre-processing; Kenney et al. 2008; Sakai et al. 2002; Gavazzi et al. 2003a; Cortese et al. 2006). They have also shown that within the tails of stripped gas, star formation in compact HII regions occurs in some but not in all objects (Gavazzi et al. 2001; Yoshida et al. 2008; Hester et al. 2010; Fumagalli et al. 2011a; Fossati et al. 2012; Boissier et al. 2012; Yagi et al. 2013; Kenney et al. 2014; Boselli et al. 2016a, 2018 – paper III). The removal of the gas affects the activity of star formation of galaxies on different timescales that depend on the perturbing mechanism (Larson et al. 1980; Boselli et al. 2006, 2016b; Bekki 2009, 2014; McGee et al. 2009; Cen 2014; Fillingham et al. 2015; Rafieferantsoa et al. 2015). The distribution and the morphology of the star-forming regions within galaxies is also tightly connected to the perturbing mechanisms (increases in the nuclear star formation activity and asymmetric distributions of star-forming regions are typical in gravitational interactions, radially truncated star-forming discs in interactions with the ICM, and fainter star forming discs in starvation, Kennicutt & Keel 1984; Barton et al. 2000; Boselli et al. 2006; Ellison et al. 2008; Woods et al. 2010; Scudder et al. 2012; Patton et al. 2011, 2013). All these pieces of evidence underline the power of NB $H\alpha$ imaging data in identifying the dominant perturbing mechanism in dense environments.

Many questions, however, remain unanswered due to the lack of systematic studies of the ionised diffuse gas through optical emission lines. This leaves many diagnostics that are key to the study of environmental processes nearly unexplored. Combined with multifrequency data, optical NB observations are crucial for identifying environment-induced effects on the different gaseous components and, ultimately, understanding the impact on star formation activity, stellar populations, and the fate of the stripped material. The main questions that a deep, complete, homogeneous $H\alpha$ survey of a nearby cluster will answer are:

1. What fraction of galaxies shows signs of perturbation as a function of galaxy mass and local density? What fraction of galaxies are perturbed by gravitational interactions or interactions with the ICM?
2. How efficiently is the gas stripped in the different phases during the interaction with the surrounding environment? How quickly does the gas change phase once it has been removed from the galaxy disc?
3. What are the ionising sources for the $H\alpha$-emitting gas (i.e. galactic or extraplanar HII regions, thermal conduction, turbulence, MHD waves, etc.)?
4. How is the nuclear and disc star formation activity of galaxies perturbed during the interaction? At which point in the

Table 1. Properties of the different Virgo cluster substructures.

Substructure	RA J2000	Dec J2000	Dist Mpc	Ref.	$< vel >$ km s^{-1}	σ km s^{-1}	Ref.	R_{200} Mpc	M_{200} $M_\odot \times 10^{14}$	Ref.	ρ_{ICM} cm^{-3}	T_{ICM} keV	Ref.	Central
Cluster A	187.71	12.39	16.5	1, 2	955	799	3	1.55	1.4–4.2	4–9	2.0×10^{-3}	2.3	10, 11	M87
Cluster B	187.44	8.00	23	1	1134	464	3	0.96	1	9				M49
Cluster C	190.85	11.45	16.5	1	1073	545	3	0.66–1.15	0.35–1.85	12, 13				M60
W cloud	185.00	5.80	32	1	2176	416	3	0.50–0.88	0.15–0.83	12, 13				NGC4261
W′ cloud	186.00	7.20	23	1	1019	416	3	0.50–0.88	0.15–0.83	12, 13				NGC4365
M cloud	183.00	13.40	32	1	2109	280	3	0.34–0.60	0.05–0.26	12, 13				NGC4168
LVC cloud	184.00	13.40	16.5	1	85	208	3	0.25–0.44	0.02–0.11	12, 13				NGC4216

References. (1) Gavazzi et al. (1999); (2) Mei et al. (2007); (3) Boselli et al. (2014a,b,c); (4) Nulsen & Böhringer (1995); (5) Girardi et al. (1998); (6) Schindler et al. (1999); (7) McLaughlin (1999); (8) Urban et al. (2011); (9) Ferrarese et al. (2012); (10) Böhringer (2005), priv. comm.; (11) Böhringer et al. (1994); (12) derived using the M_{200} vs. σ relation given in Biviano et al. (2006); (13) derived using the M_{200} vs. σ relation given in Evrard et al. (2008).

interaction is the star formation activity stopped: i.e. was the quenching rapid?

Within this framework, our team has recently been awarded 50 nights of telescope time at the Canada–France–Hawaii Telescope (CFHT) to map the whole Virgo cluster region within one virial radius (∼104 deg^2) with MegaCam using a newly commissioned NB $H\alpha$+[NII] filter[1]. This project, called VESTIGE (A Virgo Environmental Survey Tracing Ionised Gas Emission[2]), is one of the three large projects selected for the 2017–2019 observing campaigns at the CFHT. At the time of writing, after the decommissioning of SUPRIME Cam from Subaru, there is no large telescope with wide-field capability other than the CFHT equipped with $H\alpha$ NB imaging filters (at redshift 0 or above) anywhere in the world. The principal aim of this survey is to study the effects of the environment on galaxy evolution through the observation, analysis, and modelling of the ionised gas phase of the interstellar medium (ISM) of galaxies stripped during their interaction with the hostile Virgo cluster.

In this first paper we describe the survey design and the observing strategy, and we present the scientific motivations for this project. We also report on the status of the survey after the first semester of observations. The paper is structured as follows: in Sect. 2 we describe the Virgo cluster. In Sect. 3 we give the motivations, the instrumental set-up, and the design of the survey, as well as the observing strategy. In Sect. 4 we describe the data processing and in Sect. 5 we explain how the full set of data will be made available to the community. In Sect. 6 we describe the observations obtained in the 2017A semester for a 4×1 deg^2 strip across the core of the cluster. The scientific objectives of the survey are described in Sect. 7, while in Sect. 8 we present the synergy with other projects and we list the planned follow-up observations necessary for a full exploitation of the data. Throughout VESTIGE (unless otherwise stated in individual publications) we use a flat ΛCDM cosmology with $H_0 = 70$ km s^{-1} Mpc^{-1}, $\Omega_m = 0.3$, and $\Omega_\Lambda = 0.7$.

2. The Virgo cluster: A unique laboratory for environmental studies

The Virgo cluster is the richest cluster of galaxies within 35 Mpc. It is located at a distance of 16.5 Mpc (Gavazzi et al. 1999; Mei et al. 2007; Blakeslee et al. 2009) and has a total mass of $M_{200} = (1.4–4.2) \times 10^{14}\ M_\odot$ (Nulsen & Böhringer 1995; Girardi et al. 1998; Schindler et al. 1999; McLaughlin 1999; Urban et al. 2011; see Table 1), where M_{200} is the total mass within the radius in which the mean mass density is 200 times the critical cosmic mass density. With thousands of member galaxies lying at an almost equal distance and spanning all known morphological types, Virgo has historically played a key role in studies of how galaxies form and evolve in dense environments (e.g. Boselli & Gavazzi 2006). Virgo is composed of a primary virialised system (subcluster A) dominated by quiescent early-type galaxies, and by several smaller substructures falling onto the main cluster and dominated by late-type systems (Binggeli et al. 1987; Gavazzi et al. 1999; Solanes et al. 2002; Boselli et al. 2014a). The physical properties of late-type galaxies vary dramatically from the periphery (where galaxies are virtually identical to unperturbed field objects in terms of gas content and star formation activity) to the cluster core (dominated by highly perturbed systems deprived of their gas and dust reservoir and with a significantly reduced star formation activity; Kennicutt 1983; Cayatte et al. 1990; Solanes et al. 2001; Vollmer et al. 2001; Gavazzi et al. 1998, 2002a,b, 2005, 2006, 2013; Cortese et al. 2010a, 2012; Boselli et al. 2014a,c, 2016b). A wealth of observational evidence consistently indicates that Virgo is a young cluster still in formation (Tully & Shaya 1984; Gavazzi et al. 1999; Karachentsev & Nasonova 2010; Karachentsev et al. 2014; Sorce et al. 2016), and many individual member galaxies have been identified that highlight the various mechanisms by which environment can influence galaxy evolution (e.g. Vollmer 2003; Kenney et al. 2004; Vollmer et al. 2004; Boselli et al. 2005, 2006, 2016a; Haynes et al. 2007; Crowl & Kenney 2008; Abramson et al. 2011). Virgo is thus an ideal laboratory for studying (at high resolution) the perturbing mechanisms that shaped galaxy evolution.

The development of wide-field, ground- and space-based facilities has made Virgo accessible for blind surveys at different wavelengths, from the X-ray to the UV, visible, near- and far-IR, and radio, allowing astronomers to map at exquisite sensitivity and angular resolution the different constituents of galaxies (e.g. stars, cold gas in the atomic and molecular phase, ionised and hot gas, dust, magnetic fields) and the ICM (see Sect. 8). At the distance of Virgo, the typical 1–10″ resolution achieved by these surveys corresponds to ∼0.1–1 kpc and thus perfectly matches that of the most recent cosmological hydrodynamic simulations. Moreover, the dwarf galaxy population is accessible down to a stellar mass $M_{star} \sim 10^5\ M_\odot$ (NGVS, Ferrarese et al. 2016; Roediger et al. 2017). Virgo is thus the ideal target to extend the stellar mass dynamic range sampled

[1] Hereafter we will refer to the $H\alpha$+[NII] band simply as $H\alpha$, unless otherwise stated.
[2] http://mission.lam.fr/vestige/

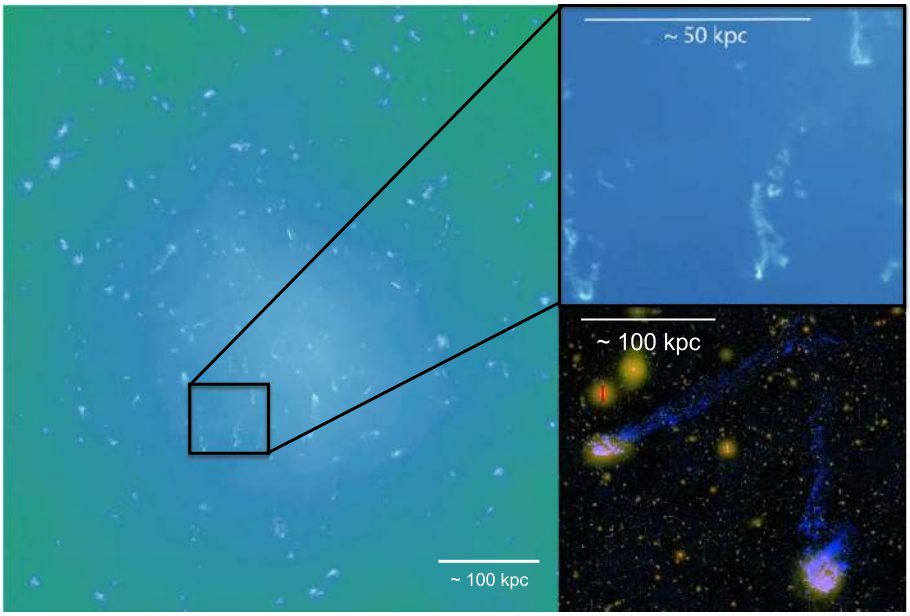

Fig. 1. Predictions for the gas distribution within a cluster of galaxies derived from the Illustris simulations (http://www.illustris-project.org/explorer; Nelson et al. 2015). Tails of stripped gas that are ~50 kpc long (*upper right panel*) are expected to be associated with most of the simulated cluster galaxies. Once stripped from galaxies and injected into the hot (10^7–10^8 K) ICM, the gas is ionised by heat conduction, turbulence, MHD waves and extraplanar star formation in the tails. It then becomes visible in deep, wide-field NB $H\alpha$ imaging. Some gas associated to star forming regions within the galactic disc can also be stripped in its ionised phase. Tails of ionised gas similar to those predicted by the simulations are indeed observed in the $H\alpha$ continuum-subtracted image of the two galaxies CGCG 97-73 and 97-79 in A1367 obtained with Suprime-Cam at the Subaru telescope ($10' \times 10'$) (Boselli & Gavazzi 2014; Yagi et al. 2017). Similar tails of ionised gas will be detected by VESTIGE.

by SDSS and other local surveys by nearly two orders of magnitude. Since it is spiral-rich, it is also better suited than more distant relaxed clusters, such as Coma, for identifying galaxies being transformed by their environments. Furthermore, Virgo has physical properties (dynamical mass, gas temperature and density) significantly different from those encountered in other nearby clusters such as Coma, A1367, and Norma, and thus can be used to extend previous studies to less extreme but more frequent and representative over-dense regions in the local Universe. For these reasons Virgo is, without question, the most thoroughly studied cluster of galaxies in the Universe, and remains the best target at low-redshift for a systematic study of the different perturbing mechanisms acting on galaxies in dense environments.

3. VESTIGE: A deep $H\alpha$ survey of the Virgo cluster

A systematic $H\alpha$ survey of Virgo is imperative if we are to understand the effects of the environment on galaxy evolution. VESTIGE has been designed to detect the low-surface-brightness tails of ionised gas observed in a handful of nearby cluster galaxies or predicted by hydrodynamic simulations to be the smoking gun of ongoing gas stripping (Tonnesen & Bryan 2010). VESTIGE will thus produce the definitive dataset against which to compare and test cosmological models of galaxy formation (Fig. 1). Compared to previous observations, which have so far targeted only a few, subjectively selected galaxies, VESTIGE will provide dramatic improvements in depth (~100× in luminosity for point sources), surface-brightness sensitivity (~30×), angular resolution (~3× in seeing), and sky coverage (~100×). Equally important, the survey will open many synergistic opportunities with planned and ongoing Virgo surveys at other wavelengths.

3.1. CFHT and MegaCam

The observations are carried out using MegaCam, a wide-field optical imager mounted on the prime focus of the 3.6 m CFHT Boulade et al. (2003). The focal ratio of the camera is F/3.77. MegaCam is composed of 40 back-illuminated 2048×4096 pixels CCDs, with a pixel size of 0.187 arcsec on the sky and a typical read noise of ~5 e pixel^{-1}. Their typical efficiency at 6563 Å is 77%. The inner 36 CCDs cover a rectangular field of view of 0.96×0.94 deg^2 in size, while the remaining (unvignetted) CCDs are located at the RA edges of the camera (see Fig. 3 in Ferrarese et al. 2012). The gaps between the different CCDs are either 13″ or 80″ wide due to the camera design.

3.2. The narrow-band $H\alpha$ filter

The observations employ the newly commissioned $H\alpha$ NB filter (MP9603). The filter bandpass measured for a F/8 focal ratio at a temperature of 20 °C covers the range $6538 < \lambda < 6644$ Å (central wavelength λ = 6591 Å, $\Delta\lambda$ 106 Å, with a typical transmissivity of 93%). The transmissivity curves of NB interferential filters change slightly with focal ratio and temperature. A blueshift of the central wavelength is expected when going from a parallel to a converging beam (the shift is non-linear), with a typical blueshift of 0.25 Å deg^{-1} expected for decreasing temperature. A decrease of the focal ratio and of the temperature also induce a very small decrease of the peak transmissivity and a slight broadening of the filter. Given that the observations are carried out in spring time, the typical temperature at the telescope is $T \sim 0$ °C, corresponding to ~5 Å blueshift. Adding an extra ~5 Å blueshift for changing the focal F/8 to F/3.77, the expected blueshift of the central wavelength during observing conditions

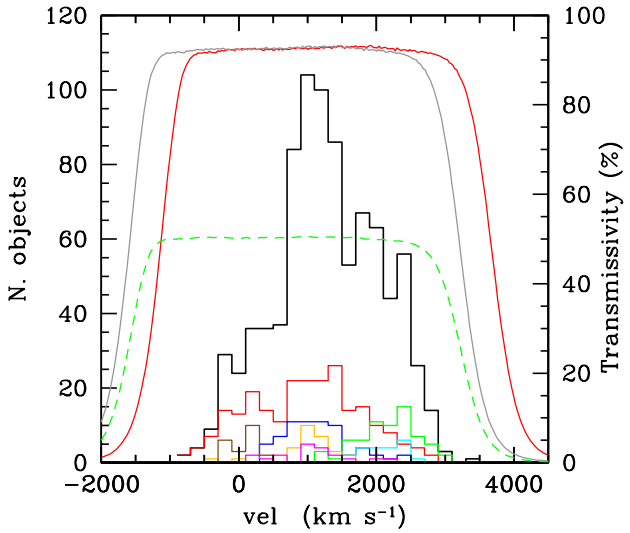

Fig. 2. Velocity distribution of galaxies within the VESTIGE footprint (black histogram) is compared to the transmissivity of the $H\alpha$ NB filter as measured in laboratory (red solid line) or expected for the typical spring observing conditions ($T = 0\,^{\circ}$C; grey solid line). The green dashed line shows the combined transmission for mirrors, optics, filter, and detectors. The velocity distribution of galaxies located within the different subclouds of the cluster defined as in Boselli et al. (2014a) are given with the coloured histograms: red – cluster A, blue – cluster B, green – W cloud, orange – W′ cloud, cyan – M cloud, magenta – cluster C, brown – low velocity cloud.

is of ∼10 Å. If we do not consider any extra marginal variation of the transmissivity curve, the NB filter covers the velocity range $-1140 < cz < +3250$ km s^{-1} for the $H\alpha$ line, and is thus perfectly suited for the velocity range of galaxies within the cluster (Binggeli et al. 1987; Boselli et al. 2014a), as depicted in Fig. 2. The filter width also brackets the two [NII] lines at λ 6548 Å and 6583 Å.

3.3. Survey geometry, exposure times, and achieved depth

Virgo is located between 12 h < RA < 13 h and 0 ° < Dec < 18°. NGVS catalogued ≃3700 Virgo cluster member galaxies within the VESTIGE footprint, out of which ∼550 are blue, presumably star-forming systems (Ferrarese et al., in prep.) as depicted in Fig. 3.

The primary goal of VESTIGE is the detection of low-surface-brightness features such as those observed in a few cluster galaxies (Gavazzi et al. 2001; Sun et al. 2007; Kenney et al. 2008; Yagi et al. 2010; Fossati et al. 2012; Boselli et al. 2016a) or predicted by hydrodynamic simulations (Roediger & Hensler 2005; Tonnesen & Bryan 2009, 2010). Such features have a typical angular size of ∼20 arcmin and a surface brightness of $\Sigma(H\alpha) \sim 1$–2×10^{-18} erg s^{-1} cm^{-2} arcsec^{-2} and thus require a sensitivity ∼60× fainter than those reached in previous observations of Virgo galaxies using 2m-class telescopes.

The total integration time of VESTIGE was determined after the pilot observations of NGC 4569 made in 2015 (Boselli et al. 2016a). The total integration time was set to 7200 s and of 720 s in the NB and broad-band r filters, respectively. Observations in the broad-band filter are necessary for the subtraction of the stellar continuum. The integration time in the broad-band, which is approximately 14 times wider than the NB, has been chosen to reach approximately the same sensitivity. The observations carried out at the CFHT during the 2017A semester in dark/grey time have shown that the typical sensitivity of VESTIGE is $\Sigma(H\alpha) \sim 1.5 \times 10^{-17}$ erg s^{-1} cm^{-2} arcsec^{-2} (1σ) at full resolution (0.187 arcsec pixel), and $\Sigma(H\alpha) \sim 2 \times 10^{-18}$ erg s^{-1} cm^{-2} arcsec^{-2} (1σ) once the data are smoothed to an angular resolution of ∼3 arcsec suitable for the detection of extended sources. The images gathered in semester 2017A have also been used to estimate empirically the 90% completeness limit (5σ level) for point sources. Our limiting magnitudes were computed via simulations of point-like populations, modeled with a Gaussian profile with full width at half maximum ($FWHM$) = 0.7″, in the magnitude range $23.0 \leq m_{\rm AB} \leq 28.0$, and randomly distributed on the images. We then carried out the photometry as for the real sources with SExtractor and analysed, as a function of the magnitude, the recovery fraction of the synthetic population for the subsample of objects characterised by signal-to-noise ratio $(S/N) \geq 5$. The limit of completeness was then defined as the magnitude for which 90% of the input objects were retrieved. We found $m(\mathrm{NB}\ H\alpha)_{\rm lim} = 24.4$ AB mag, corresponding to $f(H\alpha)_{\rm lim} = 4 \times 10^{-17}$ erg s^{-1} cm^{-2}, and $m(r)_{\rm lim} = 24.5$ AB mag, for the narrow- and broad-band images, respectively (see Table 2). The sensitivity for point sources is close to the detection limit for PNe, that in Virgo is at $f(H\alpha)$ $\sim 3 \times 10^{-17}$ erg s^{-1} cm^{-2} as derived from their $H\alpha$ luminosity function (Ciardullo 2010), and is sufficient to sample the bright end of the $z = 4.4$ Lyα luminosity function which has a characteristic flux of $f(Ly\alpha) = 2$–4×10^{-17} erg s^{-1} cm^{-2} (Ouchi et al. 2008; Cassata et al. 2011).

To conclude, each sky position is observed with a 7200 s integration in $H\alpha$ and 720 s integration in the r-band. Each exposure, in both $H\alpha$ and r, is divided into 12 exposures optimally dithered to cover the CCD gaps and minimise the possible contamination from the reflections of bright stars (see below).

3.4. Data acquisition and observing strategy

The data are acquired following the Elixir-LSB pointing strategy successfully developed for the NGVS and optimised for the best characterisation of the sky background and the detection of extended low-surface-brightness features. The strategy requires an uninterrupted sequence of seven single exposures of contiguous fields to minimise any variation in the background illumination. The observations taken during a pilot project have shown that, in the NB, flat fielding can be severely affected by the reflection of bright stars (∼7 mag) both within and outside the MegaCam field of view (see Fig. 4). These reflections are more important in the NB than in the broad-band filters. The bright stars located within the MegaCam field produce circular annuli around the star with properties depending on the brightness and on the position of the star within the field. Since these reflections depend on the optical configuration of the camera, the MegaCam community is trying to model these reflections with the purpose of defining and producing dedicated pipelines able to remove them from the images (Regnault et al., in prep.). The reflections due to stars outside the MegaCam field of view produce ghosts that change significantly according to the relative position of the camera and of the star. These ghosts can be easily removed using a median stacking of dithered images provided that each single frame is taken at significantly different positions (see Fig. 4). We thus adopt an observing pattern defined to cover the same sky region in 12 different frames taken after a large dithering of 15 arcmin in RA and 20 arcmin in Dec. Each single exposure is of 600 s in the NB and 60 s in the r-band. To map the full NGVS footprint, VESTIGE requires 1419 single pointings in each

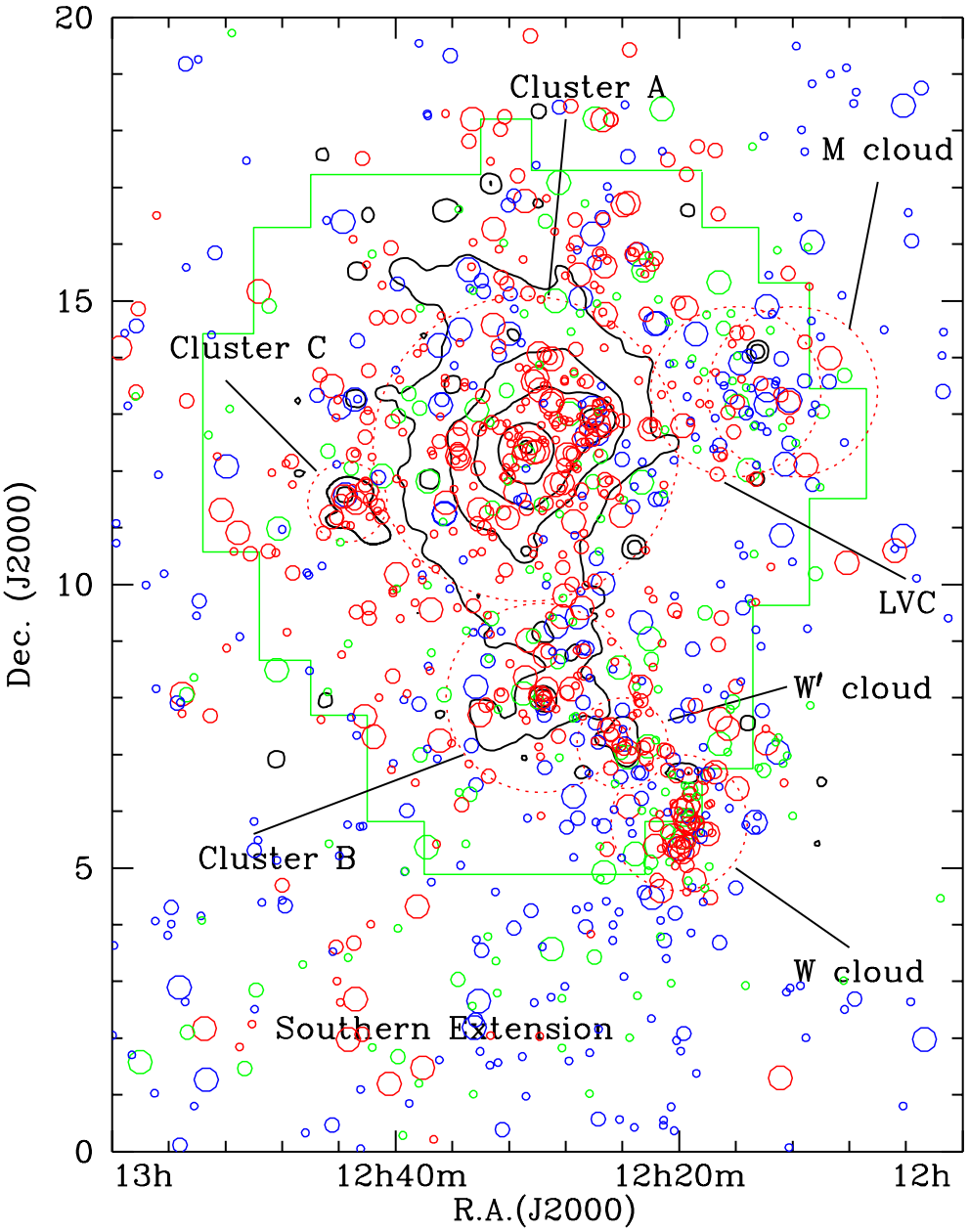

Fig. 3. Virgo cluster region mapped by VESTIGE. The complete blind survey covers the inner 104 deg^2 (green footprint), the same region mapped by NGVS (Ferrarese et al. 2012). The black contours indicate the X-ray emission of the diffuse gas of the cluster obtained by ROSAT (Böhringer et al. 1994), the large red dotted circles indicate the different substructures of the cluster, while the red, green, and blue empty circles indicate early-type galaxies, transition type galaxies, and star-forming systems, respectively, with sizes depending on their stellar mass (big for $M_{\rm star} > 10^{9.5}\,M_{\odot}$, medium for $10^{8.5} < M_{\rm star} \leq 10^{9.5}\,M_{\odot}$, small for $M_{\rm star} \leq 10^{8.5}\,M_{\odot}$) as defined in Boselli et al. (2014a).

Table 2. Sensitivity of VESTIGE.

Band	Point source	Units	Extended sources	Units
r (MP9602)	24.5	AB mag (5σ)	25.8	AB mag arcsec^{-2} (1σ)
NB $H\alpha$ (MP9603)	24.4	AB mag (5σ)	25.6	AB mag arcsec^{-2} (1σ)
$f(H\alpha)$	4×10^{-17}	erg s^{-1} cm^{-2} (5σ)	2×10^{-18}	erg s^{-1} cm^{-2} arcsec^{-2} (1σ)^a

Notes. $^{(a)}$After smoothing the data to ~3 arcsec resolution.

filter, or equivalently 203 observing blocks of 7 frames each. This particular observing pattern covers the gaps between the different CCDs composing MegaCam. With this pattern, most of the Virgo cluster will be covered by 12 independent frames, while only a small fraction coinciding with the gaps of the CCDs by 6, 8, 9 or 10 frames, as depicted in Fig. 5.

Pilot observations undertaken in 2015 and 2016 indicate that with single exposures of 600 s in the NB and 60 s in the r-band the frames are background limited in both bands (≃195 ADUs in r and 141 ADUs in NB taken in dark time). Short exposures (60 s in $H\alpha$ and 6 s in r) might be necessary whenever the analysis of the deep images reveals saturation in the nucleus of bright

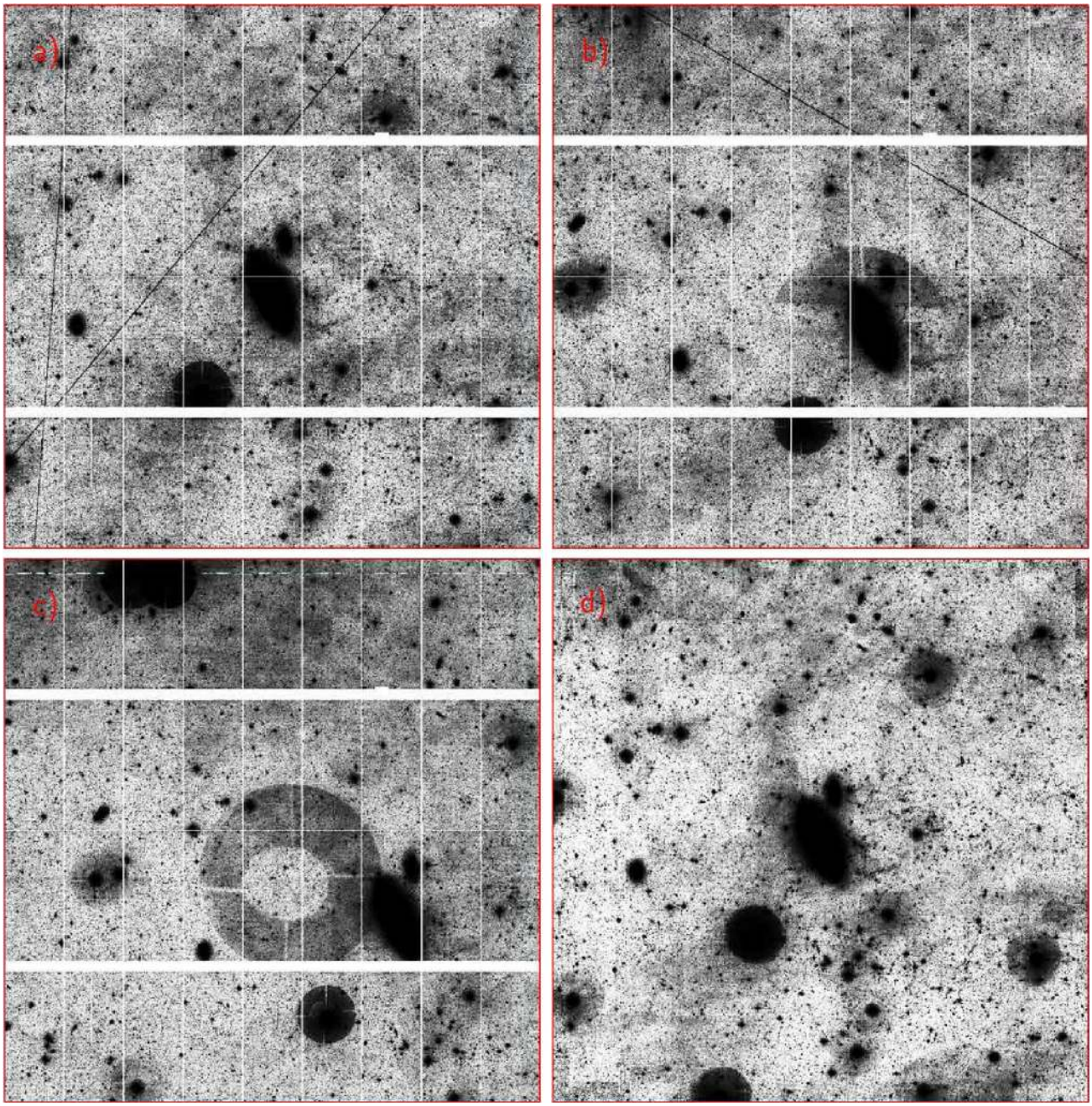

Fig. 4. *Panels a–c*: megaCam images of the galaxy NGC 4569 obtained during three different pointings reduced using the standard Elixir pipeline. A prominent ghost due to the reflection of a star is evident in two of them (*panels b and c*). Given their different position on the frame, the ghosts are efficiently removed after stacking seven independent frames reduced using Elixir-LSB (*panel d*: the grid pattern in the periphery of this frame is due to undersampled regions).

galaxies. Based on the NGVS data, we expect approximately 80 galaxies to saturate in the long exposures.

During the observing campaign of spring 2017 (semester 2017A) 244 pointings in the *r*-band (17% of the full survey) and 268 (19%) in the NB filter were acquired.

3.5. Image quality

Given the extended, low-surface-brightness nature of the ionised gas tails, no strong constraints on the seeing conditions are needed for the survey. However, given the exceptional imaging quality of the CFHT, the observations will be gathered in subarcsecond conditions. Figure 6 shows the seeing distribution for the single exposures in the $H\alpha$ and *r*-band filters obtained during the 2017A semester and 2015 and 2016 pilot observations. The median seeing in the two filters is 0.65 and 0.66 arcsec, respectively.

4. Data processing

VESTIGE benefits from the extensive machinery developed to support the NGVS survey completed with the same instrument. Accurate flat-fielding is done using Elixir-LSB, while global astrometric solutions, image stacking, and source catalogues are generated by a modified version of MegaPipe (Gwyn 2008).

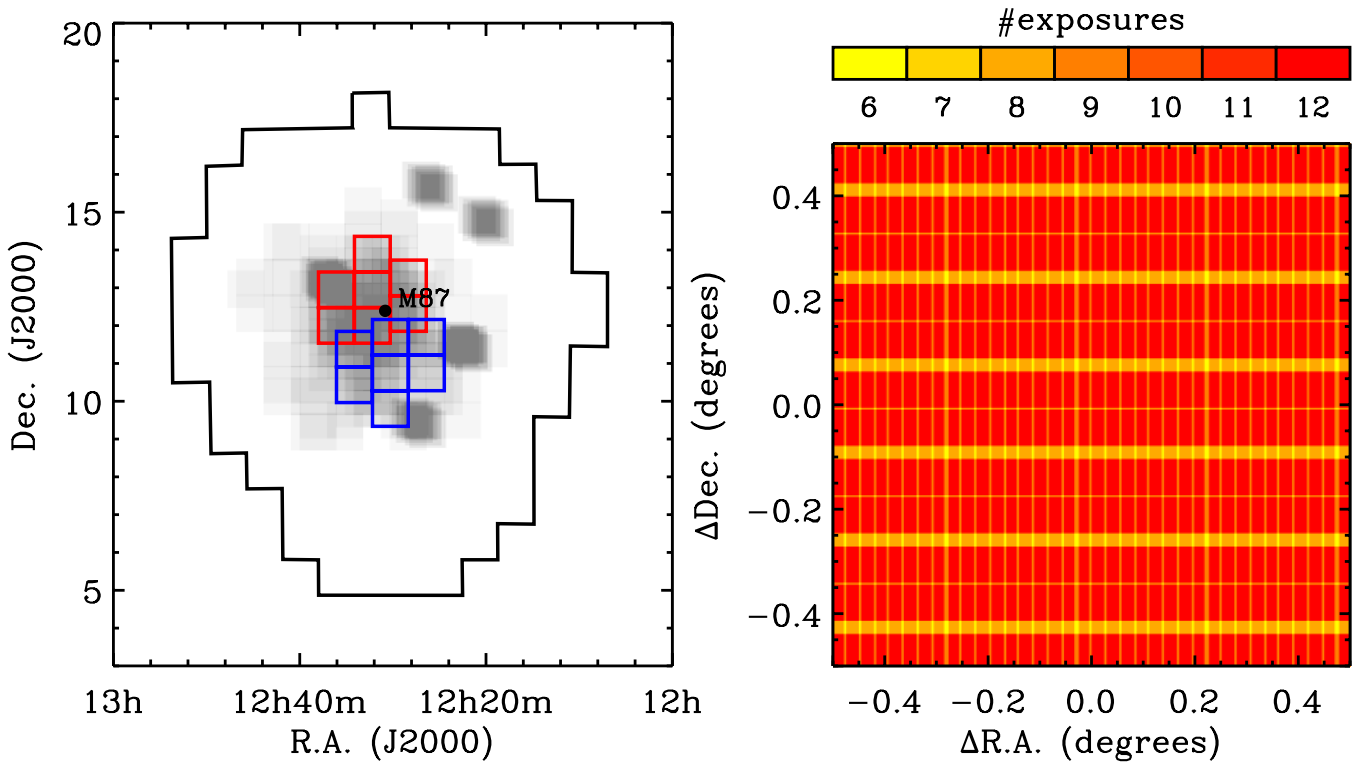

Fig. 5. *Left*: VESTIGE maps of the 104 deg^2 within the NGVS footprint with 1419 independent frames in both the $H\alpha$ NB and the r-band filters. To optimise the flat-fielding using the Elixir-LSB pipeline, the observations are gathered within an observing block of seven concatenated and adjacent frames, as depicted by the red and blue footprints here taken as two examples. The total number of observing blocks requested to cover the whole cluster is 203. Those obtained after the 2017A observing campaign are marked in grey with brightness increasing with the number of completed exposures (0 = white, 12 = dark grey). The dark regions in the outskirts of the clusters are the pilot observations completed in 2015 and 2016. *Right*: each sky region is covered by 12 independent frames dithered by 20 arcmin in right ascension (RA) and 15 arcmin in declination (Dec). This large dithering secures the sampling of the gaps between the different CCDs of MegaCam with a minimum of six exposures.

4.1. Elixir-LSB

The MegaCam images are reduced with Elixir-LSB (Ferrarese et al. 2012), an upgrade of the Elixir (Magnier & Cuillandre 2004) pipeline specifically developed within the NGVS collaboration to detect extended low-surface-brightness features associated to cluster galaxies, whose scales of $\lesssim$20 arcmin do not exceed the MegaCam field of view. This specific pipeline has been designed to remove any possible residual large-scale structure in the sky background, including the low-level diffuse Galactic emission extending all over the VESTIGE footprint (see Sect. 7.2.1). Elixir-LSB can be applied whenever the different frames are acquired under a similar background illumination, for example, within a concatenated cycle of seven independent exposures (see Sect. 3.4). The images must be background dominated, as is the case for the VESTIGE data in both the broad- and NB filters. The Elixir-LSB pipeline performs bad-pixel masking, bias and overscan corrections, and flat-fielding.

4.2. Astrometric calibration

While the MegaPipe pipeline now uses *Gaia* (Perryman et al. 2001) as an astrometric reference frame, for consistency with NGVS the VESTIGE data were astrometrically calibrated using the NGVS data (Ferrarese et al. 2012) as a reference, the latter being calibrated on the SDSS. There are small but significant astrometric shifts relative to *Gaia*, on the order of 100 mas or less. The internal astrometric residuals, on the other hand, are typically 20–40 mas.

4.3. Photometric calibration

The VESTIGE data is bootstrapped from Pan-STARRS PS1 photometry (Magnier et al. 2013) which is accurate to within $\leq$0.005 mag (Finkbeiner et al. 2016) and is sufficiently deep to provide a large number of common stars per field to minimise random errors per source. We first apply a $\sim$0.2 mag flat field radial correction from the centre to the edges to take into account the different transmissivity of the camera. This correction has been determined after the repeated observation of a nearby cluster of stars observed in different positions across the field. The magnitudes of stars in each VESTIGE image are transformed from the PS1 filter system into the MegaCam filter system and then used as in-field standards. The transformations are derived by first computing the transmission functions of the PS1 and MegaCam passbands (including the reflectance of the primary mirrors, the camera optics, the quantum efficiency of the CCDs and the transmittance of the filters themselves). These total transmission functions are multiplied by stellar spectra from both the HST CALSPEC spectra collection[3] and Pickles (1998).

The transformations are as follows:

$$r_{\rm MP9602} = r_{\rm PS1} + 0.00020 - 0.01700x + 0.00554x^2 - 0.000692x^3, \quad (1)$$

$$H\alpha_{\rm MP9603} = r_{\rm PS1} + 0.08677 - 0.29983x + 0.15859x^2 - 0.055190x^3, \quad (2)$$

[3] http://www.stsci.edu/hst/observatory/crds/calspec.html

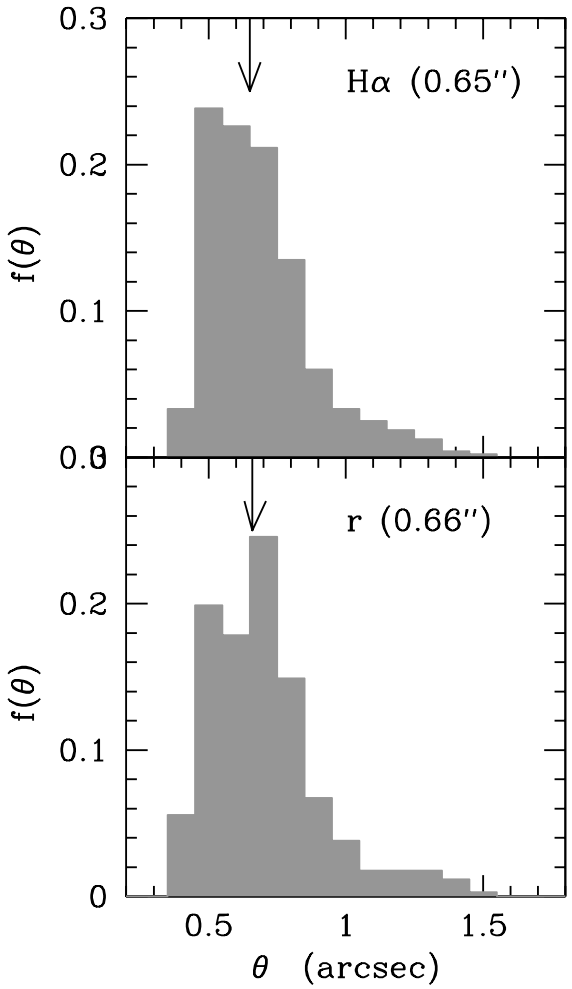

Fig. 6. Seeing distribution in the $H\alpha$ NB (*upper panel*) and r-band (*lower panel*) filters determined from the single images gathered during the 2017A observing campaign and in the 2015 and 2016 pilot observations. The vertical arrows indicate the median values.

where $x = g_{PS1} - r_{PS1}$.

The MegaCam instrumental magnitudes are measured through circular apertures that increase in size with seeing. The aperture is such that, for point sources, the measured flux is equivalent to that measured by a Kron magnitude such as SExtractor's `MAG_AUTO`.

For each exposure, a single zero-point is determined for the entire mosaic. In practice there are small variations in the zero-point across the focal plane ($\lesssim$0.03 mag), however because of the nature of the low-surface-brightness background subtraction, these are not corrected. The zero-points are determined for each exposure independently. Comparing photometry from overlapping images indicates that the zero-points are self-consistent to about 0.01 mag. We also derived a set of relations similar to Eqs. (1) and (2) using a procedure to transform SDSS magnitudes into MegaCam magnitudes to check the consistency on the photometry between the two surveys. The SDSS zero-points were consistent with the PS1-derived zero-points of VESTIGE to within 0.01 mag.

4.4. Stacking

The calibrated images are resampled onto a pixel grid matching the NGVS image footprints using SWarp[4] and the astrometric solution. The images are scaled according to the photometric solution. The resampled, scaled images are combined using an artificial skepticism algorithm (Stetson 1987)[5]. As with the NGVS data products, the resulting stacks have a zero point of 30.0 mag, such that AB magnitudes are given by:

$$m_{AB} = -2.5 \times \log(CNTS) + 30.0. \quad (3)$$

4.5. $H\alpha$ fluxes and equivalent widths

$H\alpha$ fluxes and equivalent widths are determined following standard procedures such as those described in Kennicutt et al. (2008). Given the depth of the present survey, the accuracy on the $H\alpha$ flux determination depends on an accurate subtraction of the stellar continuum. Given the width of the r filter ($\lambda_c = 6404$ Å; $\Delta\lambda = 1480$ Å) and the slight difference in the peak wavelength of the two bands, the derivation of the stellar continuum in the NB from the r-band depends on the spectral properties of the emitting source (Spector et al. 2012). Using several hundred thousand unsaturated stars detected in the science frames observed during the pilot observations and in the 2017A observing run, we were able to calibrate an empirical relation between the colour of the stars and the normalisation factor:

$$\frac{r}{H\alpha} = r - 0.1713 \times (g - r) + 0.0717. \quad (4)$$

We then apply this normalisation pixel by pixel on the stacked frame before the subtraction of the stellar continuum. The $g - r$ colour map of any target can be derived using the g-band frame taken with MegaCam during the NGVS survey (Ferrarese et al. 2012). To avoid the introduction of any extra noise in the sky regions, where there is no stellar continuum, this colour-dependent normalisation is applied only whenever the signal in the r- and g-bands has a S/N above a given threshold. The methodology used to derive fluxes and equivalent widths from the VESTIGE NB images will be extensively described in a dedicated publication (Fossati et al., in prep.).

5. Data access

All data and data products will be stored at, and distributed by, the Centre of Astrophysical Data in Marseille (CeSAM) through a dedicated web-page[6], as successfully done for several projects of which some team members are leaders (The *Herschel* Reference Survey[7]; GUViCS[8]; NGVS[9] and GOLDMine[10]). The stored data will include the fully reduced, stacked images in both the NB and r-band, as well as the continuum-subtracted frames. It will also include the full catalogues of point sources in both bands.

6. First results

6.1. Comparison with previous observations

A huge amount of pointed shallow NB $H\alpha$ imaging data (Young et al. 1996; Macchetto et al. 1996; Koopmann et al. 2001;

[4] http://www.astromatic.net/software/swarp

[5] http://ned.ipac.caltech.edu/level5/Stetson/Stetson_contents.html

[6] http://mission.lam.fr/vestige/

[7] http://hedam.lam.fr/HRS/

[8] http://galex.lam.fr/guvics/index.html

[9] http://www.cadc.hia.nrc.gc.ca/en/community/ngvs

[10] http://goldmine.mib.infn.it/

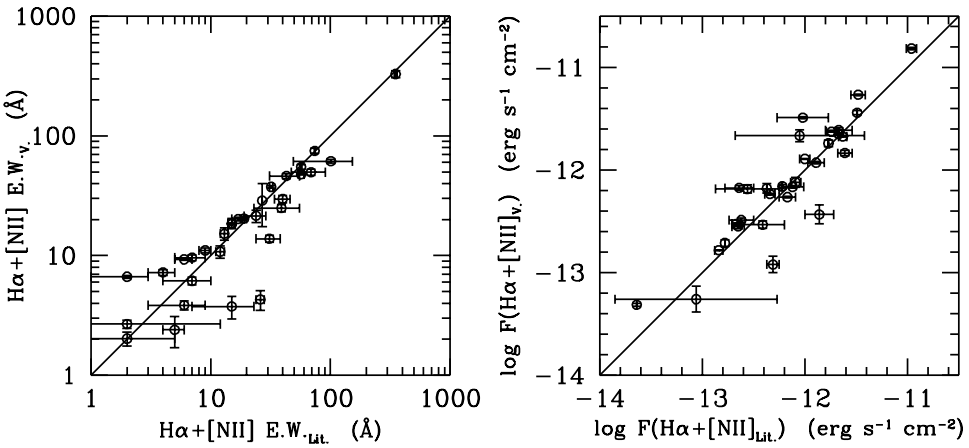

Fig. 7. Comparison of the $H\alpha$ equivalent width (*left*) and fluxes (*right*) of the Virgo galaxies observed during the first 2017A semester of the VESTIGE survey or during the pilot projects (Y-axis) with independent measurements available in the literature (X-axis). The solid line shows the 1:1 relation.

Boselli et al. 2002b, 2015; Boselli & Gavazzi 2002; Gavazzi et al. 2002a, 2006; James et al. 2004; Sánchez-Gallego et al. 2012) to which the VESTIGE results can be compared already exists in the literature, most of which is available on the GoldMine database (Gavazzi et al. 2003b). The sky regions observed during the 2017A campaign and the pilot projects include 31 galaxies with published NB $H\alpha$ imaging data. Fluxes and equivalent widths are compared in Fig. 7. The different sets of data are consistent within 5% for the equivalent widths and 30% for the fluxes. The increase in the quality of the NB $H\alpha$ images obtained with MegaCam at the CFHT with respect to previous targeted $H\alpha$ images is spectacular, as depicted in Fig. 8.

6.2. A 4 × 1 deg^2 strip across the core of the cluster

The observations carried out during the first 2017A semester allowed us to map a large portion of the centre of the cluster. Although the current coverage does not yet reach the final sensitivity expected for VESTIGE all over the mapped region, these observations already provide the largest NB $H\alpha$ image of the Virgo cluster. Figure 9 shows a 4×1 deg^2 strip crossing the northern part of the core of the cluster from the giant elliptical galaxy M84 to NGC 4569, the most massive late-type galaxy of the cluster. Within this strip the survey reaches full sensitivity in the centre and in the eastern region, while only ∼20% in the western part. Figure 10 shows the NGVS g-band image of the same regions with overplotted $H\alpha$ contours showing emission at low-surface-brightness levels. Several spectacular features are evident in the images: extended filaments of ionised gas are visible to the west of NGC 4569 (Boselli et al. 2016a) and to the north-west of NGC 4388 (Yoshida et al. 2002). The image also shows the spectacular bridge of ionised gas of ≃215 kpc in length (in projected distance) linking M86 to NGC 4438 (Kenney et al. 2008). Tails of ionised gas are for the first time detected in NGC 4402 (undetected in the shallower data of Crowl et al. 2005 and Abramson et al. 2016), NGC 4425, and NGC 4531. The typical surface brightness of these extended features ranges from $\Sigma(H\alpha) \simeq 10^{-18}$ erg s^{-1} cm^{-2} arcsec^{-2} in NGC 4569 (measured on the deeper pilot observations of Boselli et al. 2016a), to $\Sigma(H\alpha) \simeq 6 \times 10^{-18}$ erg s^{-1} cm^{-2} arcsec^{-2} in the extended filaments of NGC4438 and M86, where the sensitivity of the survey is lower. This image witnesses a large variety of extended ionised gas morphologies, possibly caused by different hydrodynamical processes (tidal interactions in NGC 4438 and M86, ram pressure in NGC 4388, NGC 4402, NGC 4425, NGC 4531, and NGC 4569) proving that VESTIGE is a revolutionary survey in probing environmental effects in the Virgo cluster.

7. Scientific objectives

7.1. Virgo cluster science

7.1.1. The effects of the environment on galaxy evolution

We expect to detect low-surface-brightness ionised gas features extending across several tens of kpc in several late-type galaxies in the cluster and its surrounding regions. These features result from ongoing stripping processes, removing the gaseous content of star-forming galaxies as they enter the cluster. They can also occur in massive elliptical galaxies formed by major merging events (M87, Gavazzi et al. 2000; M86, Kenney et al. 2008), and in early-type dwarfs formed by quenching of low-mass star-forming systems (Boselli et al. 2008a). These processes are thought to play a key role in the transformation of star-forming galaxies into quiescent systems, and in the build-up of the red sequence (Balogh et al. 2000; Boselli & Gavazzi 2014). Identifying the exact nature (i.e. ram pressure stripping, harassment, starvation, tidal stripping) of the perturbing mechanisms as a function of environment (from the cluster core to its periphery) is crucial for constraining cosmological models of galaxy evolution. Meanwhile, gravitational perturbations such as tidal stirring and harassment are expected to perturb the gaseous and stellar components simultaneously, producing low-surface-brightness tails in both the $H\alpha$ and in the optical broad-band images. Gravitational perturbations can be identified by comparing visual signs of interactions with quantitative measurements (e.g. asymmetries – Conselice 2003; Gini coefficient – Abraham et al. 2003; M_{20} – Lotz et al. 2004) and with the distance from the closest companion (Patton et al. 2016). The dynamical interaction of the galaxy ISM with the hot ICM, on the contrary, should affect only the gaseous component (e.g. Fumagalli et al. 2014). The VESTIGE data will be used to: (1) determine the fraction of galaxies with signs of perturbation due to gravitational interactions or interactions with the ICM (Yagi et al. 2010); (2) identify and map in the cluster the transition dwarf galaxies, which are believed to be in the midst of a transformation from dwarf irregular to early-type dwarfs (Boselli et al. 2008a,b, 2014a; Côté et al. 2009; De Looze et al. 2013); (3) determine the physical extent, the density, and total mass of the gas in the ionised phase (making simple assumptions on the filling factor) and compare it to that of the other gas phases (Fossati et al. 2016; Boselli et al. 2016a); (4) identify extraplanar HII regions, possible progenitors

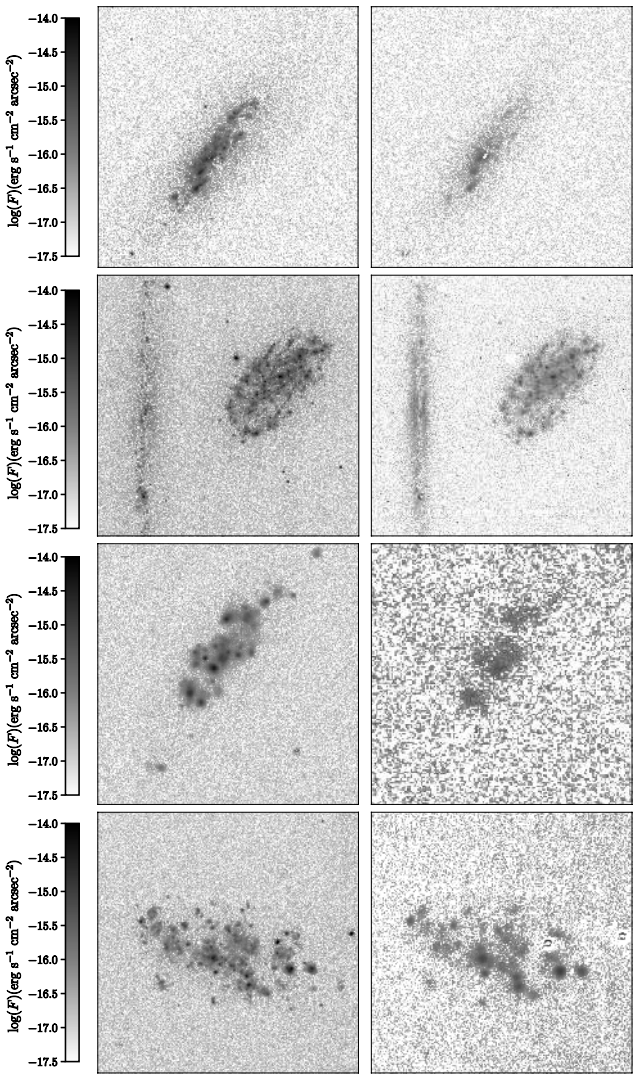

Fig. 8. Comparison of the $H\alpha$ images of the galaxies NGC4313 (SA(rs)ab:edge-on), NGC 4298 (SA(rs)c) and NGC4302 (Sc:edge-on), IC3239 (Sm) and IC 3365 (Im) obtained by VESTIGE (*left column, from top to bottom*) to those obtained with a ∼900 s on-band exposure on the 2.1 m telescope at San Pedro Martir (NGC 4313, IC3239, IC3365; Gavazzi et al. 2003b) or a 4000 s exposure on the 0.9 m telescope at Kitt Peak (NGC 4298 and 4302; Koopmann et al. 2001) (*right*).

of intracluster star clusters that can contribute to the ionisation of the gas (Fumagalli et al. 2011b; Arrigoni Battaia et al. 2012; Fossati et al. 2016; Boselli et al. 2018); and (5) compare the observations to the predictions of published (Tonnesen & Bryan 2010, 2012; Tonnesen et al. 2011; Tonnesen & Stone 2014) or upcoming hydrodynamic simulations of gas stripping developed by our team and/or presented in state-of-the-art cosmological simulations (Genel et al. 2014; Schaye et al. 2015; Barnes et al. 2017), as illustrated in Fig. 1.

7.1.2. The fate of the stripped gas in cluster galaxies

The different phases of the ISM (dust, neutral atomic and molecular gas, ionised gas, hot gas) within galaxies can be removed during interactions with the harsh cluster environment. The unprecedented multifrequency data available for Virgo, combined with tuned models of gas stripping and follow-up spectroscopic observations that we plan to obtain with SITELLE (Drissen et al. 2010) and MUSE (as in, e.g. Fumagalli et al. 2014; Fossati et al. 2016; Consolandi et al. 2017b), will be used to study the fate of this stripped material in the cluster environment. The main $H\alpha$ streams will be searched for in atomic, molecular, and X-ray gas to test the survival of cold gas in the cluster hot-gas environment (Serra et al. 2013; Jáchym et al. 2013, 2014; Verdugo et al. 2015). The data will be used to characterise the physical conditions (metallicity, density, temperature, turbulence) under which the stripped gas in its different phases (neutral, ionised, hot) can collapse to form new stars. These data are essential for constraining hydrodynamic simulations of gas stripping (Tonnesen & Bryan 2010, 2012). Simulations tailored to VESTIGE will be carried out with the 3D hydrodynamic Adaptive Mesh Refinement code FLASH (Fryxell et al. 2000) and Enzo (Bryan et al. 2014). FLASH will be updated to include a multi-phase ISM and the stellar component (Mitchell et al. 2013), as well as the thermal conduction by the hot ICM. The treatment of the different gas phases and their energetic interactions is crucial for a complete and coherent understanding of the physical process and, in turn, for constraining simulations with observational data. Systematic and complete surveys in $H\alpha$, HI, CO and X-rays are essential if we are to sample the largest possible range in the ICM, ISM, and galaxy parameter space with high statistical significance.

7.1.3. The star-forming process in nearby galaxies

Within galaxies, the $H\alpha$ emission line originates primarily from gas ionised by young and massive OB stars; it is thus an excellent tracer of ongoing star formation (Kennicutt 1998; Boselli et al. 2001, 2009; Kennicutt & Evans 2012), sensitive to stellar populations much younger than those detected in the GALEX UV bands ($H\alpha \lesssim 10$ Myr vs. $UV \lesssim 100$ Myr). VESTIGE will provide the largest and most homogeneous database ever assembled with which to study star formation down to sub-kpc scales, both in normal and perturbed galaxies and along the luminosity function, all the way down to the faintest blue compact dwarfs/HII galaxies ($L(H\alpha) \sim 10^{36}$ erg s^{-1}, equivalently to SFR $\sim 10^{-5}$ $M_\odot$ yr^{-1} when the SFR is derived using the standard calibration of Kennicutt 1998) and in virtually all star-forming systems with $M_{\rm star} \sim 10^5$ $M_\odot$. At these SFRs, we will be able to study the stochastic sampling of the IMF (Fumagalli et al. 2011a) and assess its impact on the calibration of the $H\alpha$ luminosity as a star formation tracer (Boselli et al. 2009; da Silva et al. 2014). Dust attenuation will be estimated by comparing the $H\alpha$ emission to the emission of dust in the mid- and far-infrared following standard recipes (Calzetti et al. 2010; Kennicutt et al. 2009; Zhu et al. 2008; Boselli et al. 2015) or using spatially resolved spectral energy distribution fitting analysis based on specific codes developed within our team (CIGALE, Boquien et al. 2012, 2014, 2016; Boselli et al. 2016b). The contribution of the [NII] lines can be determined using the long-slit data collected so far for the bright galaxies (Gavazzi et al. 2004; Boselli et al. 2013) or from known scaling relations (Decarli et al. 2007; Boselli et al. 2009), while possible AGN contamination can be quantified by nuclear spectroscopy available for 86% of the galaxies of the sample with $g < 17.5$ mag (≃1000 objects; Decarli et al. 2007; Gavazzi et al. 2013; SDSS). Additionally, we will be able to address the interplay between starbursts and AGN activity on a representative sample of approximately 1000 galaxies. The observed 2D properties of the star-forming activity within galaxies will also be compared to the molecular and atomic gas column densities (Boissier et al. 2001, 2003a,b, 2007, 2008) and to the predictions of multi-zone chemo-spectrophotometric models of galaxy evolution specifically tailored to take into account

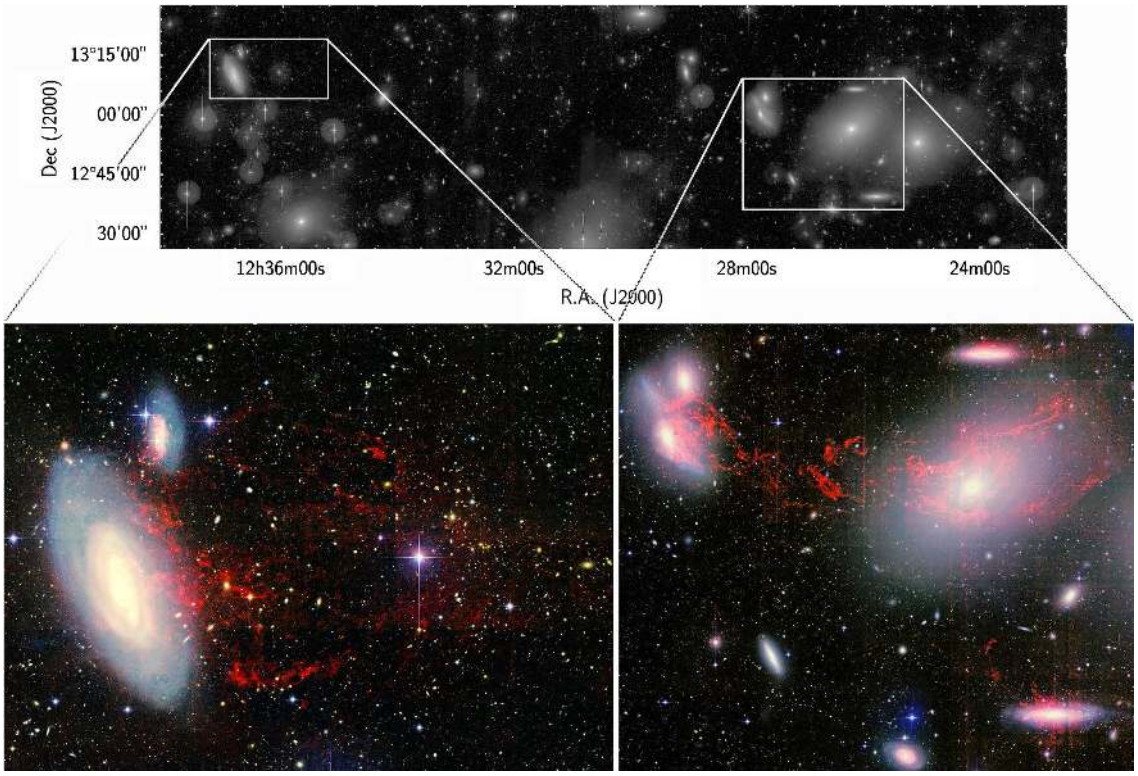

Fig. 9. *Upper panel*: g-band image of the 4×1 deg^2 (corresponding to 1.1×0.3 Mpc^2) strip of the core of the cluster north of M87. The lower panels are a magnified view of the boxed regions marked on the upper panel. They show the pseudo-colour images of NGC 4569 and IC 3583 (*lower-left panel*) and of the NGC 4438-N4388-M86 complex (*lower-right panel*) obtained combining the NGVS optical u and g in the blue channel, the r and NB in the green, and the i and the continuum-subtracted $H\alpha$ in the red.

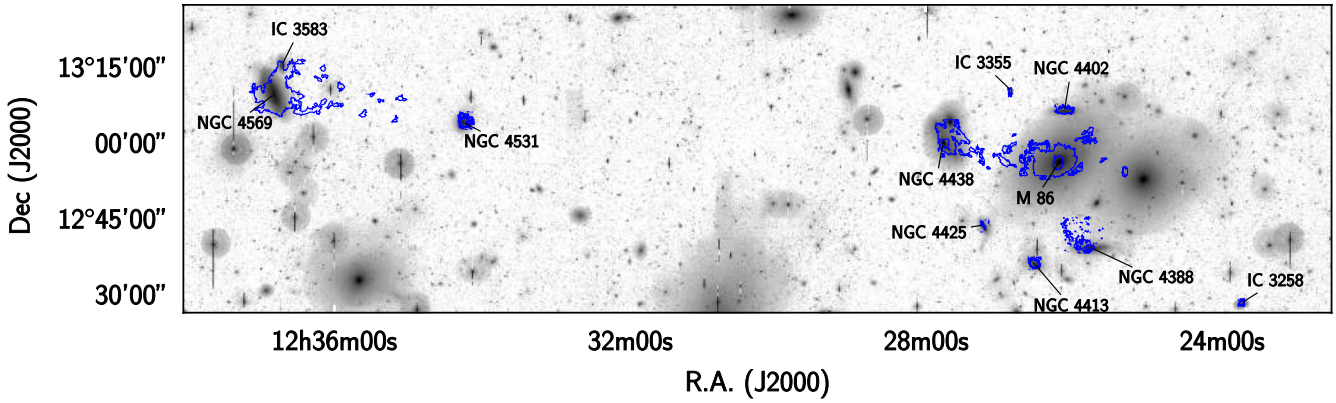

Fig. 10. Continuum-subtracted $H\alpha$ contours (blue) overplotted on the r-band image (grey) of the 4×1 deg^2 (1.1×0.3 Mpc^2) strip of the core of the cluster north of M87. Given that the survey still does not reach its full sensitivity, contours are measured at different surface brightness levels: $\Sigma(H\alpha) \simeq 10^{-18}$ erg s^{-1} cm^{-2} arcsec^{-2} for NGC 4569 and IC 3583 (from Boselli et al. 2016a), $\Sigma(H\alpha) \simeq 3 \times 10^{-18}$ erg s^{-1} cm^{-2} arcsec^{-2} for IC 3355, NGC 4388, and NGC 4531, and $\Sigma(H\alpha) \simeq 6 \times 10^{-18}$ erg s^{-1} cm^{-2} arcsec^{-2} for M86, IC 3258, NGC 4402, NGC 4413, NGC 4425, and NGC 4438.

the effects of the environment (Boselli et al. 2006, 2008a,b, 2014a).

The imprint of secular evolution on the star formation history of galaxies will be searched for by analysing the relationship between the presence of bars in the broad-band stellar images and in the NB $H\alpha$ images, extending the work of Gavazzi et al. (2015); Consolandi (2016), and Consolandi et al. (2016, 2017a) to low-surface-brightness dwarfs unreachable by the SDSS owing to its limited sensitivity and angular resolution. The data will also be compared to the predictions of chemodynamical simulations of galaxy evolution (Michel-Dansac & Wozniak 2004). The comparison between this unique set of multifrequency imaging and spectroscopic data for hundreds of resolved galaxies will be a powerful tool for reconstructing the 2D star formation history of galaxies and studying the quenching process as a function of mass, morphological type, and environment.

7.1.4. The ionised gas emission in early-type galaxies

Low levels of $H\alpha$ emission will also be detected in massive early-type galaxies (Gomes et al. 2016; Belfiore et al. 2016; Gavazzi et al. 2018), while residual star formation is expected in the core of the recently formed dE galaxies (Boselli et al. 2008a; see Fig. 11), which are often characterised by young nuclear star clusters or cores (Côté et al. 2006; Lisker et al. 2006). Given the sensitivity of the survey in terms of surface brightness, we

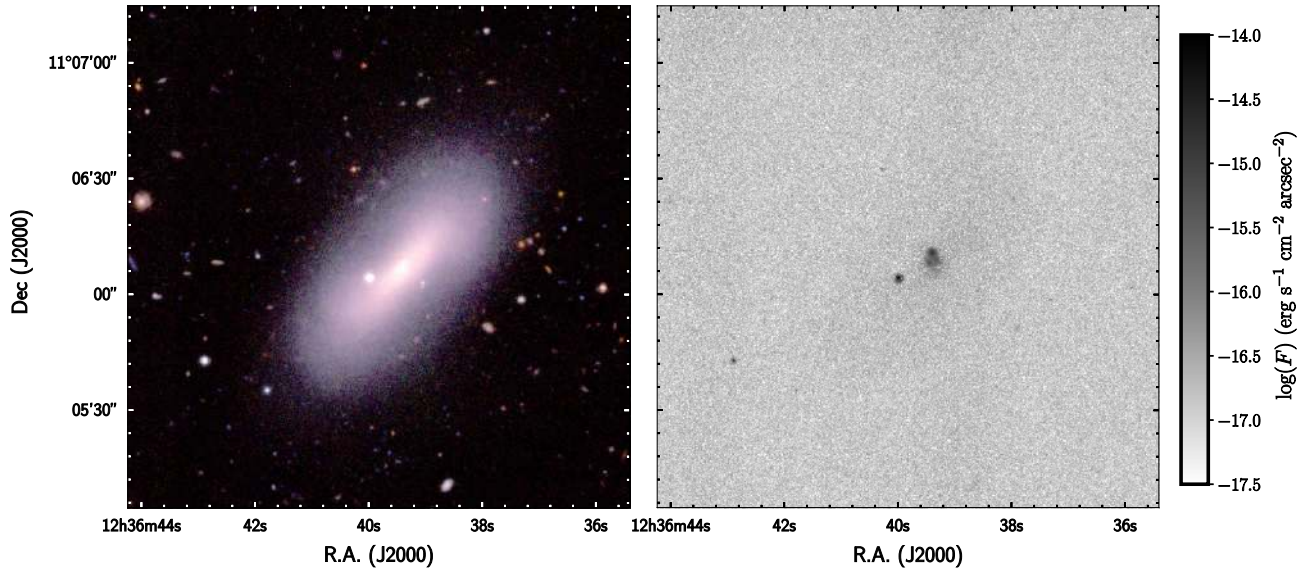

Fig. 11. NGVS *ugi* rgb colour image (*left*) and the VESTIGE continuum-subtracted $H\alpha$ image of the dwarf spheroidal galaxy (dS0(8): Binggeli et al. 1985) IC 3578 (VCC 1684). The $H\alpha$ image shows the presence of a few compact HII regions in the nucleus of the galaxy, witnessing an ongoing nuclear star forming activity.

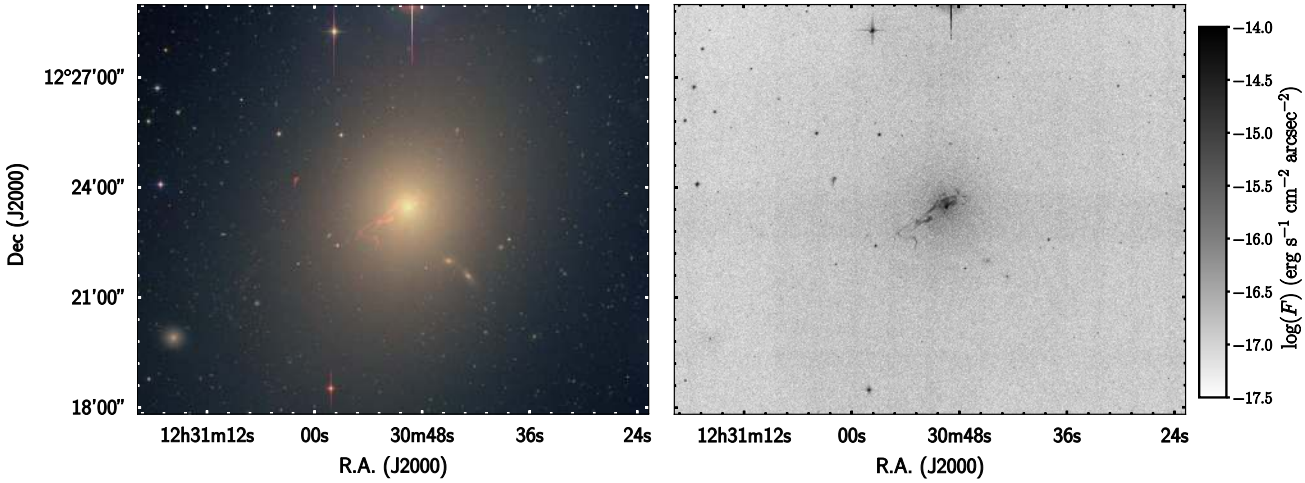

Fig. 12. *Left*: pseudo-colour image of M87 obtained combining the NGVS optical *u* and *g* in the blue channel, the *r* and NB in the green, and the *i* and the continuum-subtracted $H\alpha$ in the red. *Right*: continuum-subtracted $H\alpha$ emission of M87. Both images show the presence of prominent filaments of ionised gas extending ∼10 kpc out from the nucleus.

also expect to detect a weak diffuse emission originating from evolved stellar populations in dwarf ellipticals (Michielsen et al. 2004), or filaments of ionised gas in massive galaxies such as those observed in M87 (Sparks et al. 1993; Gavazzi et al. 2000; Fig. 12) and M86 (Trinchieri & di Serego Alighieri 1991; Kenney et al. 2008). Within the VESTIGE footprint there are 46 elliptical galaxies, 68 lenticulars, 13 S0a, and 1112 dE/dS0 galaxies catalogued in the Virgo Cluster Catalogue (Binggeli et al. 1985) with a recessional velocity $vel < 3500$ km s^{-1}, while another few thousand dwarfs, classified as Virgo members, have been detected by the NGVS survey (Ferrarese et al. 2012, 2016). VESTIGE will thus provide a unique view of the ionised gas emission properties of early-type galaxies in a complete and statistically significant sample.

7.1.5. The $H\alpha$ luminosity function

The limit in $H\alpha$ luminosity or in star formation rate (SFR) that VESTIGE will reach is approximately 100 times fainter than the limits reached by the most recent local $H\alpha$ luminosity functions (Gunawardhana et al. 2013; Fig. 13). By counting directly the number of star-forming objects in the NGVS footprints down to $M_{\rm star} \sim 10^5\,M_\odot$ we expect to detect about 500 objects. This roughly corresponds to the number derived by extrapolating the SFR luminosity function derived from the UV data (Boselli et al. 2016c) to SFR $= 10^{-5}\,M_\odot\,{\rm yr}^{-1}$, and to the number of blue galaxies detected by NGVS. This number is perfectly suited for an accurate determination of the best fitting parameters in a parametric luminosity function both within the cluster core and in the cluster periphery.

7.1.6. The $H\alpha$ scaling relations

As for the determination of the $H\alpha$ luminosity function, VESTIGE will provide us with the best sample of galaxies with $H\alpha$ data suitable for the determination of the $H\alpha$ and SFR scaling relations down to the dwarf galaxy regime, significantly increasing the most recent studies in terms of sensitivity and

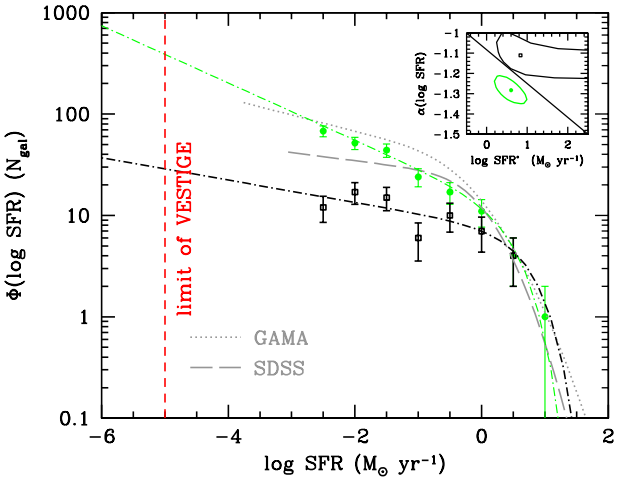

Fig. 13. Extrapolated SFR luminosity function of star-forming galaxies in the Virgo cluster periphery (green filled dots, green dot-dashed line) and in subcluster A (black open squares, black dot-dashed line) derived from the GUViCS NUV luminosity function (Boselli et al. 2016c) are compared to those derived for field galaxies by Gunawardhana et al. (2013) for the GAMA (grey dotted line) and SDSS (grey long dashed line) samples. VESTIGE will extend by two orders of magnitude any other SFR luminosity function available in the literature, sampling SFR as low as $\simeq 10^{-5}\,M_\odot\,\mathrm{yr}^{-1}$. The estimated total number of star-forming systems VESTIGE will detect will be about 500.

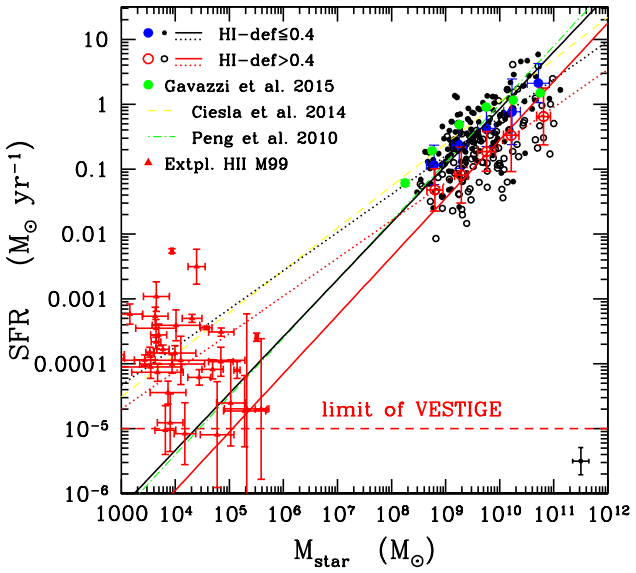

Fig. 14. Relationship between the SFR and the stellar mass (main sequence) derived for the *Herschel* Reference Survey (HRS) late-type galaxies by Boselli et al. (2015). Filled dots are for HI-normal field galaxies, empty symbols for HI-deficient Virgo cluster objects. The large filled blue and empty red circles give the mean values in different bins of stellar mass. The large green filled dots indicates the mean values of Gavazzi et al. (2015). The solid black and red lines are the bisector fit for HI-normal and HI-deficient galaxies, while the dotted lines are the linear fits. The linear best fit of Peng et al. (2010) is shown by the green dotted-dashed line, while that of Ciesla et al. (2014) by the yellow dashed line. The error bar in the lower right corner shows the typical uncertainty on the data (adapted from Boselli et al. 2015). The detection limit of VESTIGE will be $\simeq 10^{-5}\,M_\odot\,\mathrm{yr}^{-1}$. Red triangles indicate the extraplanar HII regions of NGC 4254 (M99) detected by VESTIGE and formed after a gravitational perturbation with a nearby object (paper III).

statistics (Gavazzi et al. 2013; Boselli et al. 2015). The data will be used, for instance, to extend the most recent local determinations of the star formation main sequence by three orders of magnitude (Fig. 14). These scaling relations will be determined at different clustercentric distances, from the densest regions in the core of cluster A, to the cluster periphery. Any possible observed clustercentric variation in the typical $H\alpha$ scaling relations, for the first time determined on a strong statistical basis, will be compared to the predictions of cosmological simulations and hydrodynamical models of galaxy evolution for the identification of the dominant perturbing process in rich environments.

7.1.7. The nature of almost dark galaxies

Extended HI sources without any stellar counterpart have been detected in the Virgo cluster by AGES (Taylor et al. 2012) and ALFALFA (Janowiecki et al. 2015; Cannon et al. 2015). These "dark" galaxies are particularly important since they have been proposed as a possible solution to the missing satellite problem (Bullock 2010). Their nature, however, is still poorly understood. In the most massive clouds ($\sim 10^9\,M_\odot$), the atomic gas should form molecular hydrogen, become unstable, collapse and form new stars (Taylor & Webster 2005; Burkhart & Loeb 2016). In lower-mass objects, on the contrary, the contact with the hot ICM would make the gas cloud change phase to reach the typical temperature ($T \sim 10^7$–10^8 K) of the surrounding gas (thermal evaporation, Cowie & Songaila 1977). VESTIGE might thus detect low levels of star formation within massive HI-selected dark galaxies (see Fig. 17) as well as the extended emission associated to any possible phase transition within the clouds. It can also discover new dark galaxy candidates as extended $H\alpha$ blobs without any visible stellar counterpart, for which follow-up spectroscopic observations will be required to confirm their extragalactic nature and characterise the physical properties of the ionised gas.

7.1.8. The dynamical structure of the Virgo cluster

The spectacular tails of ionised gas detected in $H\alpha$ (that can extend up to $\sim$100 kpc) trace the trajectory on the plane of the sky of galaxies that have recently entered the cluster environment (Fig. 1). Combined with radial velocities, which are available for more than 1000 objects within the selected region and velocity range ($-1000 < cz < 3500\,\mathrm{km\,s^{-1}}$), and specific numerical dynamical codes (e.g. Bovy 2015) the orientation of the extended tails of ionised gas will be used to reconstruct the orbits of individual galaxies (Vollmer 2009). These data will allow the first-ever study of the dynamical evolution of the cluster in three dimensions. Characterising the dynamical properties of the cluster is essential for a fair comparison with cosmological simulations (Vollmer et al. 2001) and, along with the physical properties of galaxies, will be of prime importance for understanding the role of pre-processing in galaxy evolution.

7.1.9. The HII region luminosity function of cluster galaxies

The sensitivity of the survey for point sources and the excellent image quality will allow us to measure the first HII region luminosity function of cluster galaxies (Kennicutt 1981). VESTIGE will be able to detect classical HII regions of luminosity $L(H\alpha) \gtrsim 10^{36}\,\mathrm{erg\,s^{-1}}$. Considering a typical seeing of 0.7 arcsec, corresponding to $\simeq$60 pc at the distance of Virgo, VESTIGE will be able to resolve only giant ($L(H\alpha) = 10^{37}$–$10^{39}\,\mathrm{erg\,s^{-1}}$)

and super giant ($L(H\alpha) \simeq 10^{39}$ erg s^{-1}) HII regions. Although still limited in terms of sensitivity and angular resolution with respect to dedicated HST studies of nearby galaxies (Scoville et al. 2001; Lee et al. 2011), or galaxies in the Local Group (Kennicutt & Hodge 1986; Hodge et al. 1990, 1999), the improvement with respect to other studies based on ground-based images (Kennicutt et al. 1989; Rand 1992; Youngblood & Hunter 1999; Thilker et al. 2002; Bradley et al. 2006) will be significant in terms of sampled range of $H\alpha$ luminosity, angular resolution, and statistics.

7.1.10. Planetary nebulae and the origin of the intracluster light

Even though planetary pebula (PN) surveys in distant galaxies focus on the [OIII] λ 5007 Å emission line due to its strength, a PN spectrum is composed of several other emission lines of which $H\alpha$ is one of the strongest (Ciardullo 2010). $H\alpha$ studies of PN systems have been limited to the local Universe and very little is known about the PN properties at this wavelength for more distant objects like Virgo cluster galaxies. Ciardullo (2010) presented the $H\alpha$ luminosity function (LF) for three Local Group galaxies showing that like the [OIII] PNLF, the $H\alpha$ LF displays a cutoff that is insensitive to stellar population. The same cutoff is also visible in the recent SITELLE data of M31 (Martin et al. 2018). At the distance of the Virgo cluster, this cutoff should be at $f(H\alpha) \simeq 3 \times 10^{-17}$ erg s^{-1} cm^{-2}. This number is very close to the detection limit of the survey ($f(H\alpha) \simeq 4 \times 10^{-17}$ erg s^{-1} cm^{-2} 90% complete at 5σ, $f(H\alpha) \simeq 2.5 \times 10^{-17}$ erg s^{-1} cm^{-2} 50% complete at 5 σ). However, given the sharp increase of the PNLF at its bright end, and the large scatter in the [OIII]/$H\alpha$ ratio observed in nearby galaxies, VESTIGE can potentially detect the brightest PNe in several tens of galaxies over the 104 deg^2 covered by the survey.

PNe will be identified using standard ($H\alpha$-r) versus $H\alpha$ colour diagrams such as the one plotted in Fig. 15 and distinguished from high-z line emitters or local HII regions from the lack of any stellar emission in the deep g and i NGVS images (Jacoby et al. 1990; Theuns & Warren 1997; Ciardullo et al. 1998; Méndez et al. 2001; see however Bacon et al. 2017).

7.2. Foreground science

7.2.1. The diffuse ionised medium of the Milky Way

The $H\alpha$ filter is sensitive to the diffuse emission from ionised gas in the Milky Way (e.g. Reynolds et al. 1998). At the high Galactic latitude of Virgo ($b \sim 74°$), the diffuse Galactic $H\alpha$ emission is ~0.1–1.0 Rayleigh (corresponding to $\Sigma(H\alpha) \sim 0.5$–5×10^{-18} erg s^{-1} cm^{-2} arcsec^{-2}) as derived by the Wisconsin $H\alpha$ Mapper (WHAM) all-sky survey (Reynolds et al. 1998, Fig. 16) and can thus be detected once the signal is appropriately smoothed. The Milky Way emission can be distinguished from large-scale fake structures in the continuum-subtracted images such as those produced by poor-quality flat-fielding or bright star halos, or from the tails of ionised gas associated with Virgo cluster galaxies, once the full mosaic of images is in hand. The $H\alpha$ emission of the Galactic halo, indeed, is expected to extend over several square degrees, leading to the formation of long and continuous tails covering several frames. For this purpose we are developing within the team a modified version of the Elixir-LSB data reduction pipeline which uses the 1° resolution WHAM map (Fig. 16) as a prior to fix a zero point for the diffuse Galactic emission over each MegaCam frame. HI and CO line

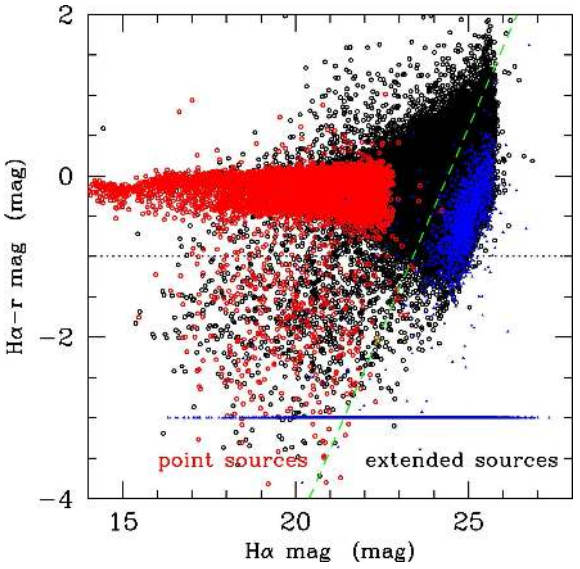

Fig. 15. $H\alpha$-r vs. $H\alpha$ colour magnitude diagram for sources in the field of NGC 4302. Red symbols are point sources, black symbols extended sources, while blue symbols show those objects detected in the NB $H\alpha$ image with a r-band detection of $S/N \leq 5$ (those with $H\alpha$-$r > -3$) or without any counterpart in the r-band ($H\alpha$-$r = -3$). The colour-dependent detection limit of VESTIGE is indicated by the green dashed line. Those sources below the colour magnitude relation, with a colour $H\alpha$-$r \leq -1$ mag (black dotted line) are line emitters and include local galaxies, PNe, and background line ([OIII], [OII], and Lyα) emitting galaxies.

widths will be used to discriminate Galactic from extragalactic emission (Cortese et al. 2010b; For et al. 2012); a technique we have already used successfully to identify and map the distribution of the scattered light produced by the Galaxy cirrus emission in GALEX far- and near-UV images of the same Virgo cluster region (Boissier et al. 2015) or that emitted by the Galactic cirrus in the far-infrared (Bianchi et al. 2017). VESTIGE will provide a substantial improvement in angular resolution with respect to WHAM, producing the first $H\alpha$ map of the Milky Way at high Galactic latitude over a ~100 deg^2 contiguous field and at a resolution of a few arcsec. It will also be complementary to shallower ($\Sigma(H\alpha) \sim 2 \times 10^{-17}$ erg s^{-1} cm^{-2} arcsec^{-2}) surveys limited to the Galactic plane (IPHAS, Drew et al. 2005; VPHAS, Drew et al. 2014; SHASSA, Gaustad et al. 2001; VTSS, Dennison et al. 1998; SHS, Parker et al. 2005). The $H\alpha$ data will be compared to those available for other components of the ISM (i.e. dust from IRAS, *Planck* and *Herschel*; HI gas from GALFA, Peek et al. 2011 and ALFALFA, Bianchi et al. 2017; scattered light from GALEX, Boissier et al. 2015) to firmly characterise the physical properties of the Milky Way's ISM at high Galactic latitudes (Boulanger et al. 1996; Lagache et al. 2000).

7.2.2. High velocity clouds, compact sources, and Galactic fountains

The HI Galactic survey done with Arecibo (GALFA-HI, Saul et al. 2012) detected 13 compact sources within the VESTIGE footprint (see Fig. 17), and others will be detected by Wallaby (Koribalski 2012). These sources have been identified as high-velocity clouds (HVC), galaxy candidates, and cold and warm low-velocity clouds (LVC). A different population of ultra-compact high-velocity clouds (UCHVC) has been also detected by ALFALFA, probably associated to very-low-mass galaxies in the Local Volume (Adams et al. 2013; Bellazzini et al. 2015).

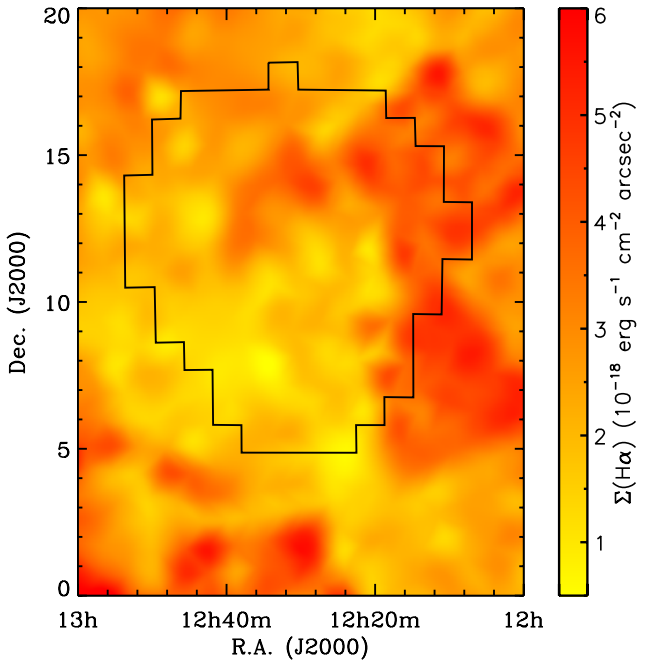

Fig. 16. Diffuse $H\alpha$ emission of the Milky Way in the direction of the Virgo cluster at an angular resolution of 1 deg, as derived from the WHAM all-sky survey (Reynolds et al. 1998).

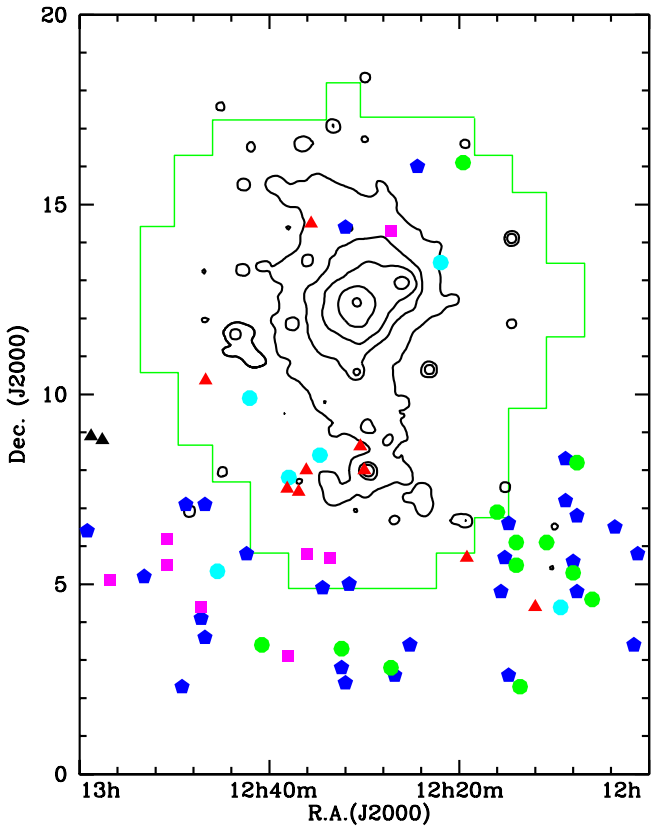

Fig. 17. Distribution of the HI compact sources detected by GALFA-HI and ALFALFA within the Virgo cluster region mapped by VESTIGE. The green footprint indicates the blind mapped region of the survey. The black contours show the X-ray emitting hot gas distribution within the cluster. Black filled triangles are HVC, red filled triangles galaxy candidates and dark galaxies (see Sect. 7.1.7), blue filled pentagons cold LVC, magenta filled squares warm LVC, green filled dots warm positive LVC (from Saul et al. 2012), while cyan filled dots UCHVC, from Adams et al. (2013).

Four of these are within the VESTIGE footprint. Given their low recessional velocity ($\lesssim$400 km s^{-1}), all these sources are potentially detectable by VESTIGE in $H\alpha$ if they contain ionised gas. All these sources will be searched for in the deep NB $H\alpha$ images. Thanks to the sensitivity of VESTIGE we expect to detect in $H\alpha$ a large fraction of HVC and LVC discovered by the HI GALFA and ALFALFA surveys, and thus significantly increase the number of objects with both atomic and ionised gas data, now limited to a handful of sources (Reynolds 1987; Haffner et al. 2001; Tufte et al. 2002). The typical peak emissivity of these features is $\simeq$0.1–0.5 Rayleigh (1 R = 5.66×10^{-18} erg s^{-1} cm^{-2} arcsec^{-2}; Reynolds 1987; Haffner et al. 2001; Tufte et al. 1998, 2002; Putman et al. 2003), and their extension is of several arcminutes (Saul et al. 2012), thus easily detectable after spatial smoothing of the VESTIGE data. The $H\alpha$ data, combined with HI and X-rays, will be used to constrain the physical properties of the clouds, study their Galactic or extragalactic origin, and quantify the escape radiation from the Galactic plane (Bland-Hawthorn & Maloney 1999; Putman et al. 2003, 2012) by comparing models to observations (Heitsch & Putman 2009; Binney et al. 2009; Wood et al. 2010; Kwak & Shelton 2010; Shelton et al. 2012).

7.3. Background science

7.3.1. High-redshift emission line galaxies

The $H\alpha$ filter combined with broad-band r or deeper NGVS images will allow us to identify strong Lyα, [OII] and [OIII] emission-line galaxies at different redshifts (z = 4.4, 0.8, 0.3), providing a unique sample of star-forming objects over $\sim$104 deg^2. Indeed, the point-source sensitivity of VESTIGE ($f(H\alpha) = 4 \times 10^{-17}$ erg s^{-1} cm^{-2}, 5σ detection limit) is comparable to the typical Lyα luminosity of z = 4.4 galaxies as derived from their Lyα luminosity function ($L^* \sim 2$–4×10^{-17} erg s^{-1} cm^{-2}; Ouchi et al. 2008; Cassata et al. 2011). It is also $\sim 2\sigma$ and $\sim 10\sigma$ deeper than the [OII] and [OIII] L^* luminosities at z = 0.8 and z = 0.3 (Ly et al. 2007; Ciardullo et al. 2013). Using model predictions for the Lyα line (Garel et al. 2015, 2016), or the luminosity functions and the number counts of [OII] and [OIII] sources derived with similar surveys of small fields (Ly et al. 2007; Hippelein et al. 2003), we estimate that $\sim 5 \times 10^4$ Lyα-, $\sim 10^5$ [OII]-, and 3×10^4 [OIII]-emitters will be detected over $\sim$104 deg^2. VESTIGE will provide an unprecedented database for characterising the bright end of the high-redshift emission line galaxies luminosity function, insensitive to cosmic variance. The data will thus be highly complementary to those obtained in deep targeted imaging and spectroscopic surveys, which are generally limited to $\lesssim$1 deg^2 (and optimised for studying the luminosity function at its faint end). At the depth of VESTIGE, the majority of the detected sources will be background objects. The continuum-subtracted image, however, will contain only local $H\alpha$ or background line emitters. High-redshift [OII] and [OIII] sources will be identified using photometric redshifts available from the NGVS (Raichoor et al. 2014), while Lyα candidates using standard ($H\alpha$-r) versus $H\alpha$ colour magnitude relations (Ouchi et al. 2008) as shown in Fig. 15, combined with other relations based on deeper g (25.9 mag) and i (25.1 mag; 10σ) NGVS images. Multi-slit wide-field spectroscopic follow-up will be carried out on a subset of the candidates to quantify the statistical accuracy in the photometric identification of the different line-emitting sources.

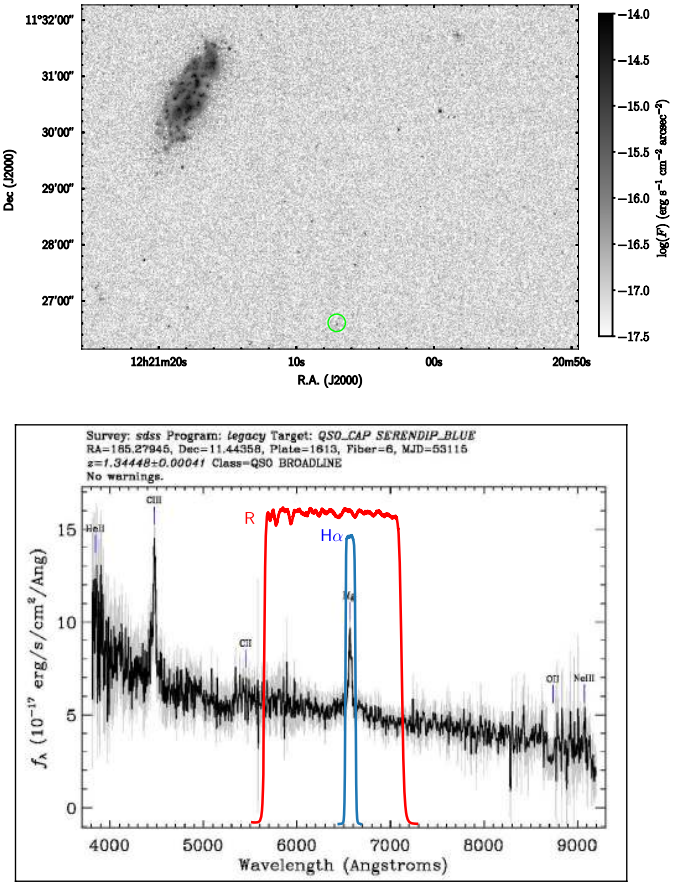

Fig. 18. *Top*: continuum-subtracted $H\alpha$ image of NGC 4294. The point source marked with a green circle indicates SDSS J122107.07+112636.8, a QSO at $z = 1.34$. *Bottom*: SDSS spectrum of this source shows a strong MgII (λ 2799 Å) emission line in the NB filter centred on the rest-frame $H\alpha$.

7.3.2. Quasi Stellar Objects (QSOs)

VESTIGE will be able to detect background quasars whenever one of their prominent emission lines falls within the NB filter. The most important emission lines in the spectrum of a quasar are [OIII] (λ 5007 Å; $z = 0.3$), $H\beta$ (λ 4861 Å; $z = 0.35$), MgII (λ 2799 Å; $z = 1.3$), CIII (λ 1908 Å; $z = 2.4$), CIV (λ 1549 Å; $z = 3.2$), and Lyα (λ 1216 Å; $z = 4.4$) (Vanden Berk et al. 2001). A typical example is the object SDSS J122107.07+112636.8, identified by SDSS as a background QSO at $z = 1.344$, detected as a strong point source in the proximity of the galaxies NGC 4294 in the continuum-subtracted $H\alpha$ image obtained during pilot observations of the VESTIGE survey (Fig. 18). The QSO has been detected thanks to a prominent MgII line emission.

7.3.3. Photometric redshifts

The r-band frames that will be gathered to subtract the contribution of the stellar continuum from the NB emission will be combined to those already available from the NGVS (*ugiz*) to increase the accuracy of the photometric redshift of background sources. At a limiting magnitude of $r \sim 25.3$ AB mag (5σ detection limit for point sources), the addition of the r-band will increase the accuracy of photometric redshifts by about 30% in the faintest objects and reduce the number of catastrophic outliers by more than a factor of two (Raichoor et al. 2014). The accuracy of the photometric redshift can be improved by the inclusion of a NB filter (COMBO-17, Wolf et al. 2003), or of other UV and near-IR photometric bands (COSMOS, Ilbert et al. 2009; NMBS, Whitaker et al. 2011). The NB filter will be crucial for the identification of overdense regions at those redshifts where it will detect the brightest emission lines of the spectrum ([OIII], $H\beta$, [OII], Lyα). Photometric redshifts are fundamental for the identification of cluster galaxies using a red sequence technique, particularly in the range $0.3 < z < 0.8$ where the r-band includes the 4000 Å break (Raichoor et al. 2014). We expect to detect approximately 4000 clusters in the $0.1 < z < 1.0$ redshift range over the 104 deg^2 covered by the NGVS survey (Olsen et al. 2007; Licitra et al. 2016), a number comparable to that discovered by the CFHTLS-Wide survey (Durret et al. 2011).

8. Synergy with other surveys and follow-up observations

VESTIGE is largely a self-contained project, but will capitalise on the extensive set of multifrequency data available for the cluster (much of it obtained by members of the VESTIGE team).

X-ray: X-ray data are necessary to trace the distribution of the hot ICM (ROSAT – Böhringer et al. 1994; ASCA – Kikuchi et al. 2000) or to quantify the physical properties of the hot gas phase in the stripped material of perturbed galaxies. There are 131 XMM observations and 365 *Chandra* observations between 0.5 deg and 8 deg from M87 in the archives. These XMM and *Chandra* observations also include many programs dedicated to Virgo spirals, such as the 2016 *Chandra* large project "Spiral Galaxies for the Virgo Cluster" led by Dr. Roberto Soria (559 ks on 52 galaxies).

UV, visible, and near-infrared: UV, visible, and near-infrared data are necessary to characterise the stripping process, identify possible ionising sources in the stripped material, and detect the optical and near-infrared counterparts of $H\alpha$ point sources. The whole Virgo cluster region has been mapped in the UV by GALEX (GUViCS – Boselli et al. 2011; Voyer et al. 2014) and in the visible by the SDSS (York et al. 2000), NGVS (Ferrarese et al. 2012), and Pan-STARRS (Magnier et al. 2013). The cluster has also been a favourite target of HST (e.g. ACSVCS, Côté et al. 2004). Near-infrared imaging data in the K_S-band over the 4 deg^2 centred on M87, and in the J- and K_S-band over ~16 deg^2 in the region between M87 and M49 have been taken during the NGVS-IR project (Muñoz et al. 2014).

Mid- and far-infrared: Infrared data are essential for correcting $H\alpha$ data for dust attenuation, for identifying the emission of the Galactic cirrus, and for a complete characterisation of the spectral energy distribution of local and background sources. Mid- (4–22 μm) and far-IR (70–500 μm) data are available from WISE (Wright et al. 2010) and from the *Herschel* blind survey HeViCS (Davies et al. 2010; Auld et al. 2013), while pointed observations of the brightest galaxies from the *Herschel* Reference Survey (HRS; Boselli et al. 2010; Ciesla et al. 2012; Cortese et al. 2014). ISO and *Spitzer* observations are available for a large fraction of the brightest galaxies (Boselli et al. 2003, 2014a; Bendo et al. 2012; Ciesla et al. 2014), while in the sub-millimetre from the *Planck* space mission (Planck Collaboration I 2014; Baes et al. 2014).

Radio millimetre and centimetre: HI and CO data are crucial for quantifying the physical properties of the cold gas phase over the disc of galaxies and within the stripped material. Radio continuum observations, sensitive to the energy loss of relativistic electrons spinning in weak magnetic fields,

will provide a further tracer of ongoing perturbations as often done through the identification of head-tail radio sources (e.g. Ulrich 1978; Sarazin 1986). The Virgo cluster region has been fully mapped in the HI line by ALFALFA (Giovanelli et al. 2005; Haynes et al. 2011) with Arecibo, while pointed high-resolution observations are available from the VLA VIVA survey (Chung et al. 2009a). The cluster will also be fully mapped by the Wallaby survey (rms ~ 1.6 mJy at 30 arcsec and 4 km s^{-1} resolution; Koribalski 2012). CO data are available for the brightest targets (Kenney & Young 1988; Young et al. 1995; Boselli et al. 1995, 2002a,b, 2014b; Helfer et al. 2003; Chung et al. 2009b). Radio continuum observations are available from the NVSS (Condon et al. 1998) and FIRST surveys (Becker et al. 1995; see Gavazzi & Boselli 1999) and will soon be available from the ASKAP EMU survey for the whole Virgo cluster region at a sensitivity of rms ~ 10 μJy beam^{-1} at 1.3 GHz with an angular resolution of 10 arcsec (Norris et al. 2011).

Spectroscopy: Multi-slit wide-field spectroscopy is necessary for the identification and the characterisation of point sources, while Integral Field Units (IFU) spectroscopy is required for the study of the physical of the perturbed galaxies and of the stripped gas. IFU data are available for a small fraction of the early-type galaxies from Guérou et al. (2015) or from the ATLAS-3D survey (Cappellari et al. 2011), and for several late-type systems from Chemin et al. (2006). High-resolution long-slit spectra are also available for a dozen dwarves (Toloba et al. 2011, 2014).

9. Summary

The Virgo Environmental Survey Tracing Ionised Gas Emission (VESTIGE) is a blind NB $H\alpha$ imaging survey of the Virgo cluster region up to its virial radius. The survey, started in 2017 and planned to run for 3 yr, is carried out with MegaCam at the Canada–France–Hawaii Telescope. VESTIGE reaches a sensitivity of $f(H\alpha) \sim 4 \times 10^{-17}$ erg s^{-1} cm^{-2} (5σ detection limit) for point sources and $\Sigma(H\alpha) \sim 2 \times 10^{-18}$ erg s^{-1} cm^{-2} arcsec^{-2} (1σ detection limit at 3 arcsec resolution) for extended sources, and will be the deepest and largest blind NB survey of a nearby cluster. The observations carried out so far of the centre of the cluster show that, at this sensitivity, VESTIGE is able to detect extended filaments of ionised gas produced by the interaction of galaxies with the surrounding environment. This survey has been designed to study the effects of the environment on galaxy evolution and will provide, for years to come, an ideal reference for comparison with cosmological models. As designed, VESTIGE will also be used to study the fate of the stripped gas in cluster objects, the star formation process in nearby galaxies of different type and stellar mass, the determination of the $H\alpha$ luminosity function and of the $H\alpha$ scaling relations down to $\sim 10^6\,M_\odot$ stellar mass objects, and the reconstruction of the dynamical structure of the Virgo cluster. Thanks to its sensitivity and large sky coverage, VESTIGE will also be used to study the HII luminosity function on hundreds of galaxies, the diffuse $H\alpha$ emission of the Milky Way at high Galactic latitude, and the properties of emission line galaxies at high redshift. The legacy value of VESTIGE is thus very high and the survey is virtually guaranteed to provide a reference for years to come.

Acknowledgements. We thank the anonymous referee for useful comments on the manuscript. We thank Jeffrey Chan for useful advice on the determination of the survey depth. We acknowledge financial support from "Programme National de Cosmologie and Galaxies" (PNCG) funded by CNRS/INSU-IN2P3-INP, CEA and CNES, France, and from "Projet International de Coopération Scientifique" (PICS) with Canada funded by the CNRS, France. This research has made use of the NASA/IPAC Extragalactic Database (NED) which is operated by the Jet Propulsion Laboratory, California Institute of Technology, under contract with the National Aeronautics and Space Administration and of the GOLD-Mine database (http://goldmine.mib.infn.it/) (Gavazzi et al. 2003b). M. B. was supported by MINEDUC-UA projects, code ANT 1655 and ANT 1656. A. L. work was supported by the Sino-French LIA-Origin joint program. M. S. acknowledges support from the NSF grant 1714764 and the Chandra Award GO6-17111X. M. F. acknowledges support by the science and technology facilities council (grant number ST/P000541/1). E. W. P. acknowledges support from the National Natural Science Foundation of China through Grant No. 11573002. K. S. acknowledges support from the Natural Sciences and Engineering Research Council of Canada (NSERC).

References

Abraham, R. G., van den Bergh, S., & Nair, P. 2003, ApJ, 588, 218
Abramson, A., Kenney, J. D. P., Crowl, H. H., et al. 2011, AJ, 141, 164
Abramson, A., Kenney, J., Crowl, H., & Tal, T. 2016, AJ, 152, 32
Adams, E. A. K., Giovanelli, R., & Haynes, M. P. 2013, ApJ, 768, 77
Albareti, F., Allende Prieto, C., Almeida A., et al. 2017, ApJS, 233, 25
Arrigoni Battaia, F., Gavazzi, G., Fumagalli, M., et al. 2012, A&A, 543, A112
Auld, R., Bianchi, S., Smith, M. W. L., et al. 2013, MNRAS, 428, 1880
Bacon, R., Conseil, S., Mary, D., et al. 2017, A&A, 608, A1
Baes, M., Herranz, D., Bianchi, S., et al. 2014, A&A, 562, A106
Balogh, M. L., Navarro, J. F., & Morris, S. L. 2000, ApJ, 540, 113
Barnes, D. J., Kay, S. T., Bahé, Y. M., et al. 2017, MNRAS, 471, 1088
Barton, E. J., Geller, M. J., & Kenyon, S. J. 2000, ApJ, 530, 660
Becker, R. H., White, R. L., & Helfand, D. J. 1995, ApJ, 450, 559
Bekki, K. 2009, MNRAS, 399, 2221
Bekki, K. 2014, MNRAS, 438, 444
Belfiore, F., Maiolino, R., Maraston, C., et al. 2016, MNRAS, 461, 3111
Bellazzini, M., Magrini, L., Mucciarelli, A., et al. 2015, ApJ, 800, L15
Bendo, G. J., Galliano, F., & Madden, S. C. 2012, MNRAS, 423, 197
Bertin, E., & Arnouts, S. 1996, A&AS, 117, 393
Bianchi, S., Giovanardi, C., Smith, M. W. L., et al. 2017, A&A, 597, A130
Binggeli, B., Sandage, A., & Tammann, G. A. 1985, AJ, 90, 1681
Binggeli, B., Tammann, G. A., & Sandage, A. 1987, AJ, 94, 251
Binney, J., Nipoti, C., & Fraternali, F. 2009, MNRAS, 397, 1804
Biviano, A., Murante, G., Borgani, S., et al. 2006, A&A, 456, 23
Blakeslee, J. P., Jordán, A., Mei, S., et al. 2009, ApJ, 694, 556
Bland-Hawthorn, J., & Maloney, P. R. 1999, ApJ, 510, L33
Böhringer, H., Briel, U. G., Schwarz, R. A., et al. 1994, Nature, 368, 828
Boissier, S., Boselli, A., Prantzos, N., & Gavazzi, G. 2001, MNRAS, 321, 733
Boissier, S., Prantzos, N., Boselli, A., & Gavazzi, G. 2003a, MNRAS, 346, 1215
Boissier, S., Monnier Ragaigne, D., Prantzos, N., et al. 2003b, MNRAS, 343, 653
Boissier, S., Gil de Paz, A., Boselli, A., et al. 2007, ApJS, 173, 524
Boissier, S., Gil de Paz, A., Boselli, A., et al. 2008, ApJ, 681, 244
Boissier, S., Boselli, A., Duc, P.-A., et al. 2012, A&A, 545, A142
Boissier, S., Boselli, A., Voyer, E., et al. 2015, A&A, 579, A29
Boquien, M., Buat, V., Boselli, A., et al. 2012, A&A, 539, A145
Boquien, M., Buat, V., & Perret, V. 2014, A&A, 571, A72
Boquien, M., Kennicutt, R., Calzetti, D., et al. 2016, A&A, 591, A6
Boselli, A. 2011, A Panchromatic View of Galaxies (Berlin: Wiley-VCH), Practical Approach Book, XVI, 324
Boselli, A., & Gavazzi, G. 2002, A&A, 386, 124
Boselli, A., & Gavazzi, G. 2006, PASP, 118, 517
Boselli, A., & Gavazzi, G. 2014, A&ARv, 22, 74
Boselli, A., Casoli, F., & Lequeux, J. 1995, A&AS, 110, 521
Boselli, A., Gavazzi, G., Donas, J., & Scodeggio, M. 2001, AJ, 121, 753
Boselli, A., Lequeux, J., & Gavazzi, G. 2002a, A&A, 384, 33
Boselli, A., Iglesias-Páramo, J., Vílchez, J. M., & Gavazzi, G. 2002b, A&A, 386, 134
Boselli, A., Sauvage, M., Lequeux, J., Donati, A., & Gavazzi, G. 2003, A&A, 406, 867
Boselli, A., Boissier, S., Cortese, L., et al. 2005, ApJ, 623, L13
Boselli, A., Boissier, S., Cortese, L., et al. 2006, ApJ, 651, 811
Boselli, A., Boissier, S., Cortese, L., & Gavazzi, G. 2008a, ApJ, 674, 742
Boselli, A., Boissier, S., Cortese, L., & Gavazzi, G. 2008b, A&A, 489, 1015
Boselli, A., Boissier, S., Cortese, L., et al. 2009, ApJ, 706, 1527
Boselli, A., Eales, S., Cortese, L., et al. 2010, PASP, 122, 261
Boselli, A., Boissier, S., Heinis, S., et al. 2011, A&A, 528, A107
Boselli, A., Hughes, T. M., Cortese, L., Gavazzi, G., & Buat, V. 2013, A&A, 550, A114
Boselli, A., Voyer, E., Boissier, S., et al. 2014a, A&A, 570, A69

Boselli, A., Cortese, L., & Boquien, M. 2014b, A&A, 564, A65
Boselli, A., Cortese, L., Boquien, M., et al. 2014c, A&A, 564, A67
Boselli, A., Fossati, M., Gavazzi, G., et al. 2015, A&A, 579, A102
Boselli, A., Cuillandre, J. C., Fossati, M., et al. 2016a, A&A, 587, A68
Boselli, A., Roehlly, Y., Fossati, M., et al. 2016b, A&A, 596, A11
Boselli, A., Boissier, S., Voyer, E., et al. 2016c, A&A, 585, A2
Boselli, A., Fossati, M., Cuillandre, J. C., et al. 2018, A&A, in press, DOI: 10.1051/0004-6361/201732410 (Paper III)
Boulade, O., Charlot, X., Abbon, P., et al. 2003, Proc. SPIE, 4841, 72
Boulanger, F., Abergel, A., Bernard, J.-P., et al. 1996, A&A, 312, 256
Bovy, J. 2015, ApJS, 216, 29
Bradley, T. R., Knapen, J. H., Beckman, J. E., & Folkes, S. L. 2006, A&A, 459, L13
Bryan, G. L., Norman, M. L., O'Shea, B. W., et al. 2014, ApJS, 211, 19
Bullock, J. S. 2010, ArXiv e-prints [arXiv:1009.4505]
Burkhart, B., & Loeb, A. 2016, ApJ, 824, L7
Byrd, G., & Valtonen, M. 1990, ApJ, 350, 89
Cassata, P., Le Fèvre, O., Garilli, B., et al. 2011, A&A, 525, A143
Calzetti, D., Wu, S.-Y., Hong, S., et al. 2010, ApJ, 714, 1256
Cannon, J. M., Martinkus, C. P., Leisman, L., et al. 2015, AJ, 149, 72
Cappellari, M., Emsellem, E., Krajnović, D., et al. 2011, MNRAS, 413, 813
Cayatte, V., van Gorkom, J. H., Balkowski, C., & Kotanyi, C. 1990, AJ, 100, 604
Cen, R. 2014, ApJ, 781, 38
Chemin, L., Balkowski, C., Cayatte, V., et al. 2006, MNRAS, 366, 812
Chung, A., van Gorkom, J. H., Kenney, J. D. P., & Vollmer, B. 2007, ApJ, 659, L115
Chung, A., van Gorkom, J. H., Kenney, J. D. P., Crowl, H., & Vollmer, B. 2009a, AJ, 138, 1741
Chung, E. J., Rhee, M.-H., Kim, H., et al. 2009b, ApJS, 184, 199
Ciardullo, R. 2010, PASA, 27, 149
Ciardullo, R., Jacoby, G. H., Feldmeier, J. J., & Bartlett, R. E. 1998, ApJ, 492, 62
Ciardullo, R., Gronwall, C., Adams, J. J., et al. 2013, ApJ, 769, 83
Ciesla, L., Boselli, A., Smith, M. W. L., et al. 2012, A&A, 543, A161
Ciesla, L., Boquien, M., Boselli, A., et al. 2014, A&A, 565, A128
Condon, J. J., Cotton, W. D., Greisen, E. W., et al. 1998, AJ, 115, 1693
Conselice, C. J. 2003, ApJS, 147, 1
Consolandi, G. 2016, A&A, 595, A67
Consolandi, G., Gavazzi, G., Fumagalli, M., Dotti, M., & Fossati, M. 2016, A&A, 591, A38
Consolandi, G., Dotti, M., Boselli, A., Gavazzi, G., & Gargiulo, F. 2017a, A&A, 598, A114
Consolandi, G., Gavazzi, G., Fossati, M., et al. 2017b, A&A, 606, A83
Cortés, J. R., Kenney, J. D. P., & Hardy, E. 2015, ApJS, 216, 9
Cortese, L., Gavazzi, G., Boselli, A., et al. 2006, A&A, 453, 847
Cortese, L., Davies, J. I., Pohlen, M., et al. 2010a, A&A, 518, L49
Cortese, L., Bendo, G. J., Boselli, A., et al. 2010b, A&A, 518, L63
Cortese, L., Bendo, G. J., Isaak, K. G., Davies, J. I., & Kent, B. R. 2010c, MNRAS, 403, L26
Cortese, L., Ciesla, L., Boselli, A., et al. 2012, A&A, 540, A52
Cortese, L., Fritz, J., Bianchi, S., et al. 2014, MNRAS, 440, 942
Côté, P., Blakeslee, J. P., Ferrarese, L., et al. 2004, ApJS, 153, 223
Côté, P., Piatek, S., Ferrarese, L., et al. 2006, ApJS, 165, 57
Côté, S., Draginda, A., Skillman, E. D., & Miller, B. W. 2009, AJ, 138, 1037
Cowie, L. L., & Songaila, A. 1977, Nature, 266, 501
Cowie, L. L., Songaila, A., Hu, E. M., & Cohen, J. G. 1996, AJ, 112, 839
Crain, R. A., Schaye, J., Bower, R. G., et al. 2015, MNRAS, 450, 1937
Crowl, H. H., & Kenney, J. D. P. 2008, AJ, 136, 1623
Crowl, H. H., Kenney, J. D. P., van Gorkom, J. H., & Vollmer, B. 2005, AJ, 130, 65
da Silva, R. L., Fumagalli, M., & Krumholz, M. R. 2014, MNRAS, 444, 3275
Davies, J. I., Baes, M., Bendo, G. J., et al. 2010, A&A, 518, L48
Decarli, R., Gavazzi, G., Arosio, I., et al. 2007, MNRAS, 381, 136
De Looze, I., Baes, M., Boselli, A., et al. 2013, MNRAS, 436, 1057
De Lucia, G., Weinmann, S., Poggianti, B. M., Aragón-Salamanca, A., & Zaritsky, D. 2012, MNRAS, 423, 1277
Dennison, B., Simonetti, J. H., & Topasna, G. A. 1998, PASA, 15, 147
Dressler, A. 1980, ApJ, 236, 351
Dressler, A. 2004, Clusters of Galaxies: Probes of Cosmological Structure and Galaxy Evolution (Cambridge: Cambridge University Press), 206
Dressler, A., Oemler, Jr., A., Couch, W. J., et al. 1997, ApJ, 490, 577
Drew, J. E., Greimel, R., Irwin, M. J., et al. 2005, MNRAS, 362, 753
Drew, J. E., Gonzalez-Solares, E., Greimel, R., et al. 2014, MNRAS, 440, 2036
Drissen, L., Bernier, A.-P., Rousseau-Nepton, L., et al. 2010, Proc. SPIE, 7735, 77350B
Durret, F., Adami, C., Cappi, A., et al. 2011, A&A, 535, A65
Ellison, S. L., Patton, D. R., Simard, L., & McConnachie, A. W. 2008, AJ, 135, 1877
Evrard, A. E., Bialek, J., Busha, M., et al. 2008, ApJ, 672, 122
Feldmeier, J. J., Ciardullo, R., Jacoby, G. H., & Durrell, P. R. 2003, ApJS, 145, 65
Ferrarese, L., Côté, P., Cuillandre, J.-C., et al. 2012, ApJS, 200, 4
Ferrarese, L., Côté, P., Sánchez-Janssen, R., et al. 2016, ApJ, 824, 10
Fillingham, S. P., Cooper, M. C., Wheeler, C., et al. 2015, MNRAS, 454, 2039
Finkbeiner, D. P., Schlafly, E. F., Schlegel, D. J., et al. 2016, ApJ, 822, 66
For, B.-Q., Koribalski, B. S., & Jarrett, T. H. 2012, MNRAS, 425, 1934
Fossati, M., Gavazzi, G., Boselli, A., & Fumagalli, M. 2012, A&A, 544, A128
Fossati, M., Fumagalli, M., Boselli, A., et al. 2016, MNRAS, 455, 2028
Fossati, M., Mendel, J. T., Boselli, A., et al., 2018, A&A, 614, A57 (Paper II)
Fryxell, B., Olson, K., Ricker, P., et al. 2000, ApJS, 131, 273
Fumagalli, M., da Silva, R. L., & Krumholz, M. R. 2011a, ApJ, 741, L26
Fumagalli, M., Gavazzi, G., Scaramella, R., & Franzetti, P. 2011b, A&A, 528, A46
Fumagalli, M., Fossati, M., Hau, G. K. T., et al. 2014, MNRAS, 445, 4335
Garel, T., Blaizot, J., Guiderdoni, B., et al. 2015, MNRAS, 450, 1279
Garel, T., Guiderdoni, B., & Blaizot, J. 2016, MNRAS, 455, 3436
Gaustad, J. E., McCullough, P. R., Rosing, W., & Van Buren, D. 2001, PASP, 113, 1326
Gavazzi, G., & Boselli, A. 1999, A&A, 343, 86
Gavazzi, G., Pierini, D., & Boselli, A. 1996, A&A, 312, 397
Gavazzi, G., Catinella, B., Carrasco, L., Boselli, A., & Contursi, A. 1998, AJ, 115, 1745
Gavazzi, G., Boselli, A., Scodeggio, M., Pierini, D., & Belsole, E. 1999, MNRAS, 304, 595
Gavazzi, G., Boselli, A., Vílchez, J. M., Iglesias-Paramo, J., & Bonfanti, C. 2000, A&A, 361, 1
Gavazzi, G., Boselli, A., Mayer, L., et al. 2001, ApJ, 563, L23
Gavazzi, G., Boselli, A., Pedotti, P., Gallazzi, A., & Carrasco, L. 2002a, A&A, 396, 449
Gavazzi, G., Bonfanti, C., Sanvito, G., Boselli, A., & Scodeggio, M. 2002b, ApJ, 576, 135
Gavazzi, G., Cortese, L., Boselli, A., et al. 2003a, ApJ, 597, 210
Gavazzi, G., Boselli, A., Donati, A., Franzetti, P., & Scodeggio, M. 2003b, A&A, 400, 451
Gavazzi, G., Zaccardo, A., Sanvito, G., Boselli, A., & Bonfanti, C. 2004, A&A, 417, 499
Gavazzi, G., Boselli, A., van Driel, W., & O'Neil, K. 2005, A&A, 429, 439
Gavazzi, G., Boselli, A., Cortese, L., et al. 2006, A&A, 446, 839
Gavazzi, G., Fumagalli, M., Fossati, M., et al. 2013, A&A, 553, A89
Gavazzi, G., Consolandi, G., Dotti, M., et al. 2015, A&A, 580, A116
Gavazzi, G., Consolandi, G., Pedraglio, S., et al. 2018, A&A, 611, A28
Geller, M. J., & Huchra, J. P. 1989, Science, 246, 897
Genel, S., Vogelsberger, M., Springel, V., et al. 2014, MNRAS, 445, 175
Giovanelli, R., Haynes, M. P., Kent, B. R., et al. 2005, AJ, 130, 2598
Girardi, M., Giuricin, G., Mardirossian, F., Mezzetti, M., & Boschin, W. 1998, ApJ, 505, 74
Gnedin, O. Y. 2003, ApJ, 589, 752
Gomes, J. M., Papaderos, P., Kehrig, C., et al. 2016, A&A, 588, A68
Guérou, A., Emsellem, E., McDermid, R. M., et al. 2015, ApJ, 804, 70
Gunawardhana, M. L. P., Hopkins, A. M., Bland-Hawthorn, J., et al. 2013, MNRAS, 433, 2764
Gunn, J. E., & Gott, III, J. R., 1972, ApJ, 176, 1
Gwyn, S. D. J. 2008, PASP, 120, 212
Haffner, L. M., Reynolds, R. J., & Tufte, S. L. 2001, ApJ, 556, L33
Haynes, M. P., Giovanelli, R., & Kent, B. R. 2007, ApJ, 665, L19
Haynes, M. P., Giovanelli, R., Martin, A. M., et al. 2011, AJ, 142, 170
Helfer, T. T., Thornley, M. D., Regan, M. W., et al. 2003, ApJS, 145, 259
Heitsch, F., & Putman, M. E. 2009, ApJ, 698, 1485
Hester, J. A., Seibert, M., Neill, J. D., et al. 2010, ApJ, 716, L14
Hippelein, H., Maier, C., Meisenheimer, K., et al. 2003, A&A, 402, 65
Hodge, P. W., Gurwell, M., Goldader, J. D., & Kennicutt, R. C., Jr. 1990, ApJS, 73, 661
Hodge, P. W., Balsley, J., Wyder, T. K., & Skelton, B. P. 1999, PASP, 111, 685
Ilbert, O., Capak, P., Salvato, M., et al. 2009, ApJ, 690, 1236
Ivezić, Ž., Lupton, R. H., Schlegel, D., et al. 2004, Astron. Nachr., 325, 583
Jáchym, P., Kenney, J. D. P., Ržuička, A., et al. 2013, A&A, 556, A99
Jáchym, P., Combes, F., Cortese, L., Sun, M., & Kenney, J. D. P. 2014, ApJ, 792, 11
Jacoby, G. H., Ciardullo, R., & Ford, H. C. 1990, ApJ, 356, 332
Janowiecki, S., Leisman, L., Józsa, G., et al. 2015, ApJ, 801, 96
James, P. A., Shane, N. S., Beckman, J. E., et al. 2004, A&A, 414, 23
Karachentsev, I. D., & Nasonova, O. G. 2010, MNRAS, 405, 1075
Karachentsev, I. D., Tully, R. B., Wu, P.-F., Shaya, E. J., & Dolphin, A. E. 2014, ApJ, 782, 4
Kauffmann, G., White, S. D. M., & Guiderdoni, B. 1993, MNRAS, 264, 201

Kauffmann, G., White, S. D. M., Heckman, T. M., et al. 2004, MNRAS, 353, 713
Kenney, J. D., & Young, J. S. 1988, ApJS, 66, 261
Kenney, J. D. P., van Gorkom, J. H., & Vollmer, B. 2004, AJ, 127, 3361
Kenney, J. D. P., Tal, T., Crowl, H. H., Feldmeier, J., & Jacoby, G. H. 2008, ApJ, 687, L69
Kenney, J. D. P., Geha, M., Jáchym, P., et al. 2014, ApJ, 780, 119
Kennicutt, Jr., R. C. 1981, ApJ, 247, 9
Kennicutt, Jr., R. C., 1983, AJ, 88, 483
Kennicutt, Jr., R. C., 1998, ARA&A, 36, 189
Kennicutt, Jr., R. C., & Hodge, P. W. 1986, ApJ, 306, 130
Kennicutt, Jr., R. C., & Keel, W. C. 1984, ApJ, 279, L5
Kennicutt, Jr., R. C., Edgar, B. K., & Hodge, P. W. 1989, ApJ, 337, 761
Kennicutt, Jr., R. C., Lee, J. C., Funes, J. G., et al. 2008, ApJS, 178, 247
Kennicutt, Jr., R. C., Hao, C.-N., Calzetti, D., et al. 2009, ApJ, 703, 1672
Kennicutt, R. C., & Evans, N. J. 2012, ARA&A, 50, 531
Kikuchi, K., Itoh, C., Kushino, A., et al. 2000, ApJ, 531, L95
Koopmann, R. A., Kenney, J. D. P., & Young, J. 2001, ApJS, 135, 125
Koribalski, B. S. 2012, PASA, 29, 359
Kwak, K., & Shelton, R. L. 2010, ApJ, 719, 523
Lagache, G., Haffner, L. M., Reynolds, R. J., & Tufte, S. L. 2000, A&A, 354, 247
Larson, R. B., Tinsley, B. M., & Caldwell, C. N. 1980, ApJ, 237, 692
Lee, J. H., Hwang, N., & Lee, M. G. 2011, ApJ, 735, 75
Licitra, R., Mei, S., Raichoor, A., et al. 2016, ApJ, 829, 44
Lisker, T., Glatt, K., Westera, P., & Grebel, E. K. 2006, AJ, 132, 2432
Lotz, J. M., Primack, J., & Madau, P. 2004, AJ, 128, 163
Ly, C., Malkan, M. A., Kashikawa, N., et al. 2007, ApJ, 657, 738
Macchetto, F., Pastoriza, M., Caon, N., et al. 1996, A&AS, 120, 463
Magnier, E. A., & Cuillandre, J.-C. 2004, PASP, 116, 449
Magnier, E. A., Schlafly, E., Finkbeiner, D., et al. 2013, ApJS, 205, 20
Martin, D. C., Fanson, J., Schiminovich, D., et al. 2005, ApJ, 619, L1
Martin, T. B., Drissen, L., & Melchior, A.-L. 2018, MNRAS, 473, 4130
McGee, S. L., Balogh, M. L., Bower, R. G., Font, A. S., & McCarthy, I. G. 2009, MNRAS, 400, 937
McLaughlin, D. E. 1999, ApJ, 512, L9
Mei, S., Blakeslee, J. P., Côté, P., et al. 2007, ApJ, 655, 144
Méndez, R. H., Riffeser, A., Kudritzki, R.-P., et al. 2001, ApJ, 563, 135
Merritt, D. 1983, ApJ, 264, 24
Meyer, M. J., Zwaan, M. A., Webster, R. L., et al. 2004, MNRAS, 350, 1195
Michel-Dansac, L., & Wozniak, H. 2004, A&A, 421, 863
Michielsen, D., de Rijcke, S., Zeilinger, W. W., et al. 2004, MNRAS, 353, 1293
Mihos, J. C., Janowiecki, S., Feldmeier, J. J., Harding, P., & Morrison, H. 2009, ApJ, 698, 1879
Mitchell, N. L., Vorobyov, E. I., & Hensler, G. 2013, MNRAS, 428, 2674
Moore, B., Lake, G., & Katz, N. 1998, ApJ, 495, 139
Muñoz, R. P., Puzia, T. H., Lançon, A., et al. 2014, ApJS, 210, 4
Nelson, D., Pillepich, A., Genel, S., et al. 2015, Astron. Comput., 13, 12
Norris, R. P., Hopkins, A. M., Afonso, J., et al. 2011, PASA, 28, 215
Nulsen, P. E. J. 1982, MNRAS, 198, 1007
Nulsen, P. E. J., & Böhringer, H. 1995, MNRAS, 274, 1093
Olsen, L. F., Benoist, C., Cappi, A., et al. 2007, A&A, 461, 81
Ouchi, M., Shimasaku, K., Akiyama, M., et al. 2008, ApJS, 176, 301
Parker, Q. A., Phillipps, S., Pierce, M. J., et al. 2005, MNRAS, 362, 689
Patton, D. R., Ellison, S. L., Simard, L., McConnachie, A. W., & Mendel, J. T. 2011, MNRAS, 412, 591
Patton, D. R., Torrey, P., Ellison, S. L., Mendel, J. T., & Scudder, J. M. 2013, MNRAS, 433, L59
Patton, D. R., Qamar, F. D., Ellison, S. L., et al. 2016, MNRAS, 461, 2589
Peek, J. E. G., Heiles, C., Douglas, K. A., et al. 2011, ApJS, 194, 20
Peng, Y.-J., Lilly, S. J., Kovač, K., et al. 2010, ApJ, 721, 193
Perryman, M. A. C., de Boer, K. S., Gilmore, G., et al. 2001, A&A, 369, 339
Pickles, A. J. 1998, PASP, 110, 863
Planck Collaboration I. 2014, A&A, 571, A1
Putman, M. E., Bland-Hawthorn, J., Veilleux, S., et al. 2003, ApJ, 597, 948
Putman, M. E., Peek, J. E. G., & Joung, M. R. 2012, ARA&A, 50, 491
Rafieferantsoa, M., Davé, R., Anglés-Alcázar, D., et al. 2015, MNRAS, 453, 3980
Raichoor, A., Mei, S., Erben, T., et al. 2014, ApJ, 797, 102
Rand, R. J. 1992, AJ, 103, 815
Reynolds, R. J. 1987, ApJ, 323, 553
Reynolds, R. J., Tufte, S. L., Haffner, L. M., Jaehnig, K., & Percival, J. W. 1998, PASA, 15, 14
Roediger, E., & Hensler, G. 2005, A&A, 433, 875
Roediger, J. C., Ferrarese, L., Côté, P., et al. 2017, ApJ, 836, 120
Sakai, S., Kennicutt, Jr., R. C., van der Hulst, J. M., & Moss, C. 2002, ApJ, 578, 842
Sánchez-Gallego, J. R., Knapen, J. H., Wilson, C. D., et al. 2012, MNRAS, 422, 3208
Sarazin, C. L. 1986, Rev. Mod. Phys., 58, 1
Saul, D. R., Peek, J. E. G., Grcevich, J., et al. 2012, ApJ, 758, 44
Schaye, J., Crain, R. A., Bower, R. G., et al. 2015, MNRAS, 446, 521
Schindler, S., Binggeli, B., & Böhringer, H. 1999, A&A, 343, 420
Scott, T. C., Cortese, L., Brinks, E., et al. 2012, MNRAS, 419, L19
Scoville, N. Z., Polletta, M., Ewald, S., et al. 2001, AJ, 122, 3017
Scudder, J. M., Ellison, S. L., Torrey, P., Patton, D. R., & Mendel, J. T. 2012, MNRAS, 426, 549
Serra, P., Koribalski, B., Duc, P.-A., et al. 2013, MNRAS, 428, 370
Shelton, R. L., Kwak, K., & Henley, D. B. 2012, ApJ, 751, 120
Skrutskie, M. F., Cutri, R. M., Stiening, R., et al. 2006, AJ, 131, 1163
Sivanandam, S., Rieke, M. J., & Rieke, G. H. 2014, ApJ, 796, 89
Solanes, J. M., Manrique, A., García-Gómez, C., et al. 2001, ApJ, 548, 97
Solanes, J. M., Sanchis, T., Salvador-Solé, E., Giovanelli, R., & Haynes, M. P. 2002, AJ, 124, 2440
Sorce, J. G., Gottlöber, S., Hoffman, Y., & Yepes, G. 2016, MNRAS, 460, 2015
Sparks, W. B., Ford, H. C., & Kinney, A. L. 1993, ApJ, 413, 531
Spector, O., Finkelman, I., & Brosch, N. 2012, MNRAS, 419, 2156
Stetson, P. B. 1987, PASP, 99, 191
Sun, M., Jones, C., Forman, W., et al. 2006, ApJ, 637, L81
Sun, M., Donahue, M., & Voit, G. M. 2007, ApJ, 671, 190
Sun, M., Donahue, M., Roediger, E., et al. 2010, ApJ, 708, 946
Taylor, E. N., & Webster, R. L. 2005, ApJ, 634, 1067
Taylor, R., Davies, J. I., Auld, R., & Minchin, R. F. 2012, MNRAS, 423, 787
Theuns, T., & Warren, S. J. 1997, MNRAS, 284, L11
Thilker, D. A., Walterbos, R. A. M., Braun, R., & Hoopes, C. G. 2002, AJ, 124, 3118
Toloba, E., Boselli, A., Cenarro, A. J., et al. 2011, A&A, 526, A114
Toloba, E., Guhathakurta, P., Peletier, R. F., et al. 2014, ApJS, 215, 17
Tonnesen, S., & Bryan, G. L. 2009, ApJ, 694, 789
Tonnesen, S., & Bryan, G. L. 2010, ApJ, 709, 1203
Tonnesen, S., & Bryan, G. L. 2012, MNRAS, 422, 1609
Tonnesen, S., & Stone, J. 2014, ApJ, 795, 148
Tonnesen, S., Bryan, G. L., & Chen, R. 2011, ApJ, 731, 98
Trinchieri, G., & di Serego Alighieri, S. 1991, AJ, 101, 1647
Tufte, S. L., Reynolds, R. J., & Haffner, L. M. 1998, ApJ, 504, 773
Tufte, S. L., Wilson, J. D., Madsen, G. J., Haffner, L. M., & Reynolds, R. J. 2002, ApJ, 572, L153
Tully, R. B., & Shaya, E. J. 1984, ApJ, 281, 31
Ulrich, M.-H. 1978, ApJ, 221, 422
Urban, O., Werner, N., Simionescu, A., Allen, S. W., & Böhringer, H. 2011, MNRAS, 414, 2101
Vanden Berk, D. E., Richards, G. T., Bauer, A., et al. 2001, AJ, 122, 549
Verdugo, C., Combes, F., Dasyra, K., Salomé, P., & Braine, J. 2015, A&A, 582, A6
Vogelsberger, M., Genel, S., Springel, V., et al. 2014, MNRAS, 444, 1518
Vollmer, B. 2003, A&A, 398, 525
Vollmer, B. 2009, A&A, 502, 427
Vollmer, B., Cayatte, V., Balkowski, C., & Duschl, W. J. 2001, ApJ, 561, 708
Vollmer, B., Balkowski, C., Cayatte, V., van Driel, W., & Huchtmeier, W. 2004, A&A, 419, 35
Voyer, E. N., Boselli, A., Boissier, S., et al. 2014, A&A, 569, A124
Yagi, M., Komiyama, Y., Yoshida, M., et al. 2007, ApJ, 660, 1209
Yagi, M., Yoshida, M., Komiyama, Y., et al. 2010, AJ, 140, 1814
Yagi, M., Gu, L., Fujita, Y., et al. 2013, ApJ, 778, 91
Yagi, M., Yoshida, M., Gavazzi, G., et al. 2017, ApJ, 839, 65
Yasuda, N., Fukugita, M., & Okamura, S. 1997, ApJS, 108, 417
York, D. G., Adelman, J., Anderson, Jr., J. E., et al. 2000, AJ, 120, 1579
Yoshida, M., Yagi, M., Okamura, S., et al. 2002, ApJ, 567, 118
Yoshida, M., Yagi, M., Komiyama, Y., et al. 2008, ApJ, 688, 918
Youngblood, A. J., & Hunter, D. A. 1999, ApJ, 519, 55
Young, J. S., Xie, S., Tacconi, L., et al. 1995, ApJS, 98, 219
Young, J. S., Allen, L., Kenney, J. D. P., Lesser, A., & Rownd, B. 1996, AJ, 112, 1903
Whitaker, K. E., Labbé, I., van Dokkum, P. G., et al. 2011, ApJ, 735, 86
Wolf, C., Meisenheimer, K., Rix, H.-W., et al. 2003, A&A, 401, 73
Wood, K., Hill, A. S., Joung, M. R., et al. 2010, ApJ, 721, 1397
Woods, D. F., Geller, M. J., Kurtz, M. J., et al. 2010, AJ, 139, 1857
Wright, E. L., Eisenhardt, P. R. M., Mainzer, A. K., et al. 2010, AJ, 140, 1868
Zhang, B., Sun, M., Ji, L., et al. 2013, ApJ, 777, 122
Zhu, Y.-N., Wu, H., Cao, C., & Li, H.-N. 2008, ApJ, 686, 155

[1] Aix-Marseille Université, CNRS, CNES, LAM (Laboratoire d'Astrophysique de Marseille), UMR 7326, 13388 Marseille, France
e-mail: alessandro.boselli@lam.fr
[2] Max-Planck-Institut für extraterrestrische Physik, Giessenbachstrasse 1, 85748 Garching, Germany
e-mail: mfossati@mpe.mpg.de
[3] Universitäts-Sternwarte München, Scheinerstrasse 1, 81679 München, Germany
[4] NRC Herzberg Astronomy and Astrophysics, 5071 West Saanich Road, Victoria, BC V9E 2E7, Canada
e-mail: laura.ferrarese@nrc-cnrc.gr.ca
[5] Università di Milano-Bicocca, Piazza della Scienza 3, 20100 Milano, Italy
[6] INAF – Osservatorio Astronomico di Brera, via Brera 28, 20159 Milano, Italy
[7] Kavli Institute for Astronomy and Astrophysics, Peking University, Beijing 100871, PR China
[8] Department of Physics and Astronomy, University of Waterloo, Waterloo, ON N2L 3G1, Canada
[9] Department of Physics & Astronomy, University of Western Ontario, London, ON N6A 3K7, Canada
[10] Unidad de Astronomía, Facultad de Ciencias Básicas, Universidad de Antofagasta, Avda. U. de Antofagasta 02800, Antofagasta, Chile
[11] Institut d'Astrophysique Spatiale, UMR 8617, Université Paris-Sud, Bâtiment 121, 91405 Orsay, France
[12] Laboratoire d'Astrophysique de Bordeaux, Université de Bordeaux, CNRS, B18N, allée Geoffroy Saint-Hilaire, 33615 Pessac, France
[13] Collège de France, 11 Pl. M. Berthelot, 75005 Paris, France
[14] LERMA, Observatoire de Paris, CNRS, PSL Research University, Sorbonne Universités, UPMC Univ. Paris 06, 75014 Paris, France
[15] IRAP, Institut de Recherche en Astrophysique et Planétologie, CNRS, 14 avenue Edouard Belin, 31400 Toulouse, France
[16] International Centre for Radio Astronomy Research, The University of Western Australia, 35 Stirling Highway, Crawley, WA 6009, Australia
[17] CEA/IRFU/SAP, Laboratoire AIM Paris-Saclay, CNRS/INSU, Université Paris Diderot, Observatoire de Paris, PSL Research University, 91191 Gif-sur-Yvette Cedex, France
[18] Université Laval, 2325, rue de l'université, Québec, QC G1V 0A6, Canada
[19] Institute for Computational Cosmology and Centre for Extragalactic Astronomy, Department of Physics, Durham University, South Road, Durham DH1 3LE, UK
[20] Department of Physics & Astronomy, McMaster University, Hamilton ON L8S 4K1, Canada
[21] Department of Astrophysics, University of Vienna, Türkenschanzstrasse 17, 1180 Vienna, Austria
[22] Australia Telescope National Facility, CSIRO Astronomy and Space Science, PO Box 76, Epping, NSW 1710, Australia
[23] Department of Physics and Astronomy, University of Victoria, PO Box 1700 STN CSC, Victoria, BC V8W 2Y2, Canada
[24] Department of Physics and Astronomy, Trent University, 1600 West Bank Drive, Peterborough, ON K9L 0G2, Canada
[25] Department of Astronomy, Peking University, Beijing 100871, PR China
[26] Laboratório de Astrofísica Teórica e Observacional, Universidade Estadual de Santa Cruz, 45650-000 Ilhéus, Brazil
[27] Institut d'Astrophysique de Paris, UMR7095 CNRS, Université P. & M. Curie, 98bis Bd. Arago, 75104 Paris, France
[28] Astronomy Centre, Department of Physics and Astronomy, University of Sussex, Falmer, Brighton BN1 9QH, UK
[29] UK Astronomy Technology Centre, Royal Observatory Edinburgh, Blackford Hill, Edinburgh EH9 3HJ, UK
[30] Osservatorio Astronomico di Cagliari, via della Scienza 5, 09047 Selargius, Cagliari, Italy
[31] Department of Physics, Royal Military College of Canada, PO Box 17000, Station Forces, Kingston, ON K7L 7B4, Canada
[32] Department of Physics, Engineering Physics, and Astronomy, Queen's University, Kingston, ON K7L 3N6, Canada
[33] Department of Physics and Astronomy, University of Alabama in Huntsville, Huntsville, AL 35899, USA
[34] Center for Computational Astrophysics, Flatiron Institute, 162 5th Avenue, New York, NY 10003, USA
[35] Observatoire Astronomique de Strasbourg, UMR 7750, 11, rue de l'Université, 67000 Strasbourg, France
[36] LUPM, Université de Montpellier, CNRS, Pl. Eugène Bataillon, 34095 Montpellier, France
[37] Canada France Hawaii Telescope Corporation, Kamuela, HI 96743, USA